Supporting Information

A Catalytic and Selective Scissoring Molecular Tool for Quadruplex Nucleic Acids.

Matteo Nadai,[§‡] Filippo Doria,[†‡] Matteo Scalabrin,[§] Valentina Pirota,[†] Vincenzo Grande,[†] Greta Bergamaschi,[†] Valeria Amendola,[†] Fernaldo Richtia Winnerdy,[‖] Anh Tuân Phan,[‖] Sara N. Richter,[§] Mauro Freccero.*[†]*

[§]Department of Molecular Medicine, University of Padua, via Gabelli 63, 35121 Padua, Italy; [†]Department of Chemistry, University of Pavia, V.le Taramelli 10, 27100 Pavia, Italy and [‖]School of Physical and Mathematical Sciences, Nanyang Technological University, Singapore 637371, Singapore.

Table of Contents.

Experimental Details and Materials:

All chemicals were purchased from Sigma-Aldrich and Alfa Aesar. DNA and RNA oligonucleotides were purchased from Sigma-Aldrich. HPLC analyses were performed on a 1260 Infinity Agilent system using a XSelect® HSS C18 analytical column (2,5µm, 4,6 x 50 mm). All purifications were performed on a 1260 Infinity Agilent system equipped with two preparative G1361A 1260 Infinity pumps and a 1260 diode array detector VL (working range: 190 - 750 nm), using a SunFire^{TM} C18 OBD^{TM} preparative column (5µm, 30 x 150 mm). Mass spectra of small molecules were recorded using a Thermo-Finnigan LCQ ADV MAX ion-trap mass spectrometer, with an ESI ion source. ^{1}H, ^{13}C, NMR spectra were recorded using a Bruker AVANCE 300 spectrometer operating at 300.13 MHz proton Larmor frequency. Data acquisition and processing were performed using a standard Bruker software package (Topspin 1.3). The potentiometric titrations were made with a Radiometer TitraLab 90 titration system. UV-Vis spectra were recorded on an Agilent 8453 diode array spectrophotometer, equipped with a thermostatic, magnetically stirred optical cell. Emission spectra were recorded on a Perkin Elmer LS 50B instrument.

Synthesis and Characterization of NDI-Cu-DETA.

The **NDI-Cu-DETA** ligand was obtained following the synthesis shown in Scheme 1, starting from 2,6-Dibromo-EtNMe$_2$ NDI **1** that was carried out as previous described.[S1]

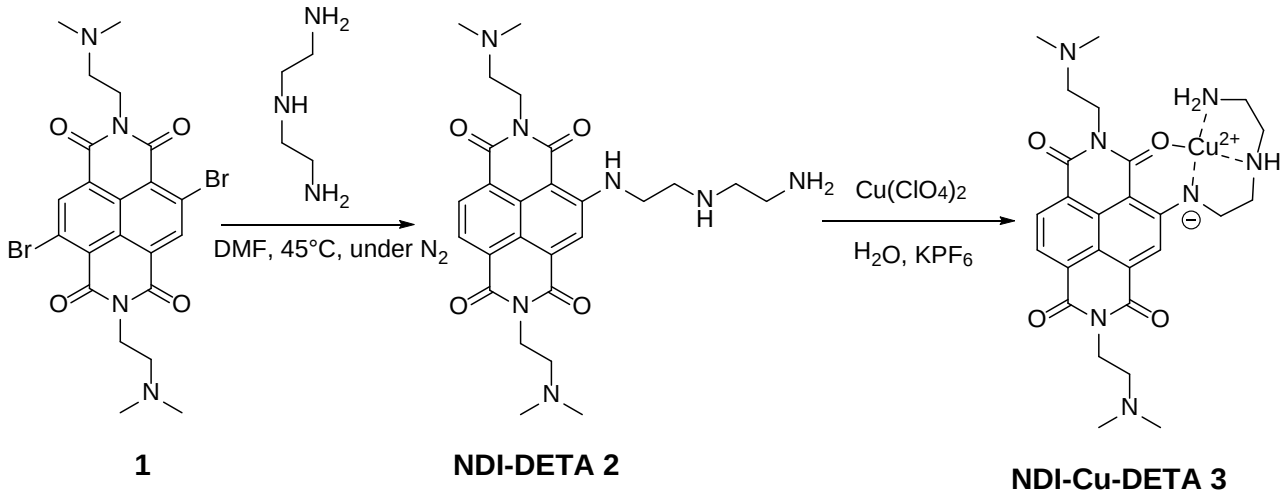

Scheme S1 - Synthesis of NDI-Cu-DETA

To obtain **NDI-DETA 2**, 0.4 g (0.727 mmol) of 1 were dissolved in DMF at 45 °C and 0.6 g (8 equiv., 5.82 mmol) of commercial diethylenetriamine were adding rapidly. The reaction mixture was stirred at 45 °C under N_2 atmosphere for 3 h following the reaction course in HPLC (t_R = 5.72 min). The crude product was cooled at r.T., protonated with the addition of a HCl (10 % v/v) and purified by preparative HPLC (t_R= 13.8 min). The compound **2** was obtained as red solid (yield 70%) and was characterized by NMR. ^{1}H-NMR (300 MHz, $CDCl_3$): δ (ppm) = 10.30 (s, NH); 8.67

(d, *J*= 7.8 Hz, 1H); 8.32 (d, *J*= 7.8 Hz, 1H); 8.2 (s, 1H); 4.36-4.29 (m, 4H); 3.7-3.68 (m, 2H); 3.10 (t, *J*= 6 Hz, 2H); 2.87-2.81 (m, 4H); 2.68-2.62 (m, 4H); 2.35 (s, 12H). ^{13}C NMR (75 MHz, $CDCl_3$) δ 165.9, 163.3, 162.9, 152.1, 131.2, 129.4, 127.7, 126.0, 124.4, 123.4, 120.0, 99.9, 56.9, 56.8, 51.9, 48.0, 45.7, 42.8, 41.6, 38.5, 38.0. Anal Calcd for $C_{26}H_{35}N_7O_4$: C, 61.28; H, 6.92; N, 19.24; O, 12.56. Found: C, 61.30; H, 6.94; N, 19.21.

The **NDI-Cu-DETA** complex **3** was obtained by dissolving 75 mg (0.115 mmol) of 2 in 10 mL of distillated water and then adding a stoichiometric amount of $Cu(ClO_4)_2$ salt leaving at r.T. under stirring for 10 min. The solution's pH was moved until 7 and a saturated solution of KPF_6 was added to induce the precipitation of a purple solid. The liquid phase was removed by centrifugation and the solid was dried and treated with cold diethyl ether (yield 80%). The **NDI-Cu-DETA 3** complex was characterized by MS direct injection in methanol (NDI-Cu-DETAH$^+$ m/z = 571NDI-Cu-DETAH_2^{2+} m/z=286).

FRET analysis

FRET assay was performed with *FAM* (6-carboxyfluorescein) 5'-end- and *Tamra* (6-carboxy-tetramethylrhodamine) 3'-end-labelled oligonucleotides. Fluorescence melting curves were determined with a LightCycler II (Roche) real-time PCR machine, using a total reaction volume of 20 µL, with 0.25 µM of tagged oligonucleotide in a buffer containing 10 mM lithium cacodylate pH 7.4 with 20, 50 or 100 mM KCl, in the presence or absence of 1.0 µM **NDI-Cu-DETA**. After a first equilibration step at 30 °C during 2 minutes, a stepwise increase of 1 °C every minute for 65 cycles to reach 95 °C was performed and measurements were made after each cycle with excitation at 470 nm and detection at 530 nm. Final analysis of the data was carried out using Excel and Sigma Plot softwares. Oligonucleotides melting was monitored observing emission of FAM, which was normalized between 0 and 1: T_m was defined as the temperature for which the normalized emission is 0.5. T_m values were mean of 2-3 experiments and ΔT_m was calculated as the difference T_m in the presence and absence of the compound.

CD analysis.

CD spectra were recorded on a Chirascan-Plus (Applied Photophysics, Leatherhead, UK) equipped with a Peltier temperature controller using a quartz cell of 5-mm optical path length and scanning a speed of 50 nm/min with a response time of 4 s over a wavelength range of 230-320 nm. The reported spectrum of each sample represents the average of 2 scans. Observed ellipticities were

converted to mean residue ellipticity (θ) = deg x cm^2 x $dmol^{-1}$ (Molar Ellipticity). Oligonucleotides were diluted from stock to the final concentration (4 μM) in Li cacodylate buffer (10 mM, pH 7.4) with different KCl concentration to maintain the initial T_m values in the 50-60 °C range, and then annealed by heating at 95 °C for 5 min, gradually cooled to room temperature. **NDI-Cu-DETA** was added at 16 μM final concentration. CD spectra were recorded after 24 h from 20°C to 95°C, with temperature increase of 5°C. T_m values were calculated according to the van't Hoff equation, applied for a two state transition from a folded to unfolded state, assuming that the heat capacity of the folded and unfolded states are equal. [S2]

Catalytic oxidation of 4-tert-butylcatechol

The catalytic oxidation of 4-tert-butylcatechol (4TBC) mediated by NDI-Cu-DETA complex was monitored through the absorption band of 4-tert butylquinone (4TBQ) at 400 nm (ε_{400nm} = 1210 $cm^{-1}M^{-1}$) [S3] and compared to that of free copper (II). The kinetic experiment was performed by dissolving 4TBC (3 mM), stock solution prepared in water to slow down the autoxidation process, in 50 mM phosphate buffer at pH 7.4 at room temperature. The absorption changes versus time were recorded after the addition of NDI-Cu-DETA (25 μM) or $CuSO_4$ (25 μM). The same study was repeated in the presence of NDI-DETA in solution environment with the copper free addition.

All measurements were performed in duplicate and all traces were corrected for 4TBC autoxidation in the same conditions. To calculated the initial rate during the first 100 s, the value of ΔA/s was divided for the quinone molar extinction coefficient and the copper complex (or free copper) concentration.

The presence of H_2O_2 (1 mM) in the mixture does not alter the kinetic profiles (data not show).

Characterization of reactive oxygen species involved.

The irreversible bleaching of para-nitrosodimethylaniline (p-NDA) was monitored spectrophotometrically as a kinetic index of ˙OH radical formation. H_2O_2 (1 mM) and ascorbate (1 mM) were added to a solution of p-NDA (6.25 μM) in 10 mM Tris-HCl buffer (pH 7.4), in presence of KCl (100 mM), in a thermostated (37 °C) 1 cm optical cells under magnetic stirring. The kinetic process was recorded from the addition of NDI-Cu-DETA complex (6.25 μM), as the last reagent, and was followed through the decrease of the optical band of p-NDA at 440 nm (ε_{440nm} = 34200 $M^{-1}cm^{-1}$).[S4]

The same experiment was recorded from the addition of NDI-Cu-DETA complex (6.25 μM) that was previously incubated with LTR-III oligomer (12.5 μM), folded into G4 structure, for 5 h.

The LTR-III oligomer was annealed by incubation at 95°C for 5 mins, in the presence of 100 mM KCl and 10 mM TRIS-HCl buffer (pH 7.4) and letting them cool down at r.t. overnight.
The kinetic process was recorded also from the addition of NDI-Cu-DETA complex (6.25 μM), as the last reagent, in a solution contained H_2O_2 (1 mM), ascorbate (1 mM), p-NDA (6.25 μM) and 100 equiv. of mannitol (0.625 mM) in 10 mM tris buffer (pH 7.4), in presence of KCl (100 mM).

DNA selective cleavage

All oligonucleotides were gel-purified before use and prepared in desalted/lyophilised form. Oligonucleotides were 5'-end-labelled with [γ- 32P]ATP by T4 polynucleotide kinase and were subsequently purified by MicroSpin G-25 columns (Amersham Biosciences, Europe), resuspended in lithium cacodylate 10 mM, pH 7.4, KCl 100 mM, heat-denatured and folded. Samples for MS characterization of cleavage products were obtained using 5'-phosphate equivalent oligonucleotides. Duplex substrate was obtained by annealing the labelled forward oligonucleotide with equimolar amounts of the reverse, partially complement cold oligonucleotide (Table S2).
Oligonucleotides (0.25 μM) were incubated with **NDI-Cu-DETA** for 24 h at 20 °C. Next they were incubated for 2.5 or 5 min at 37 °C after addition of 1 mM sodium ascorbate and 1 mM hydrogen peroxide. For mannitol treatment, 100 equivalents of mannitol were added simultaneously to **NDI-Cu-DETA,** ascorbate and hydrogen peroxide.
At the indicated time intervals, reactions were stopped adding 4 mM EDTA and samples were ethanol precipitated. In the case of piperidine treatment, samples were reacted with 1 M hot piperidine for 30 minutes, subsequently lyophilised, suspended in water and lyophilised again, and finally resuspended in formamide gel loading buffer.
Purine marker were prepared according to the Maxam and Gilbert protocol.[S5] Samples were then lyophilised, suspended in formamide gel loading buffer, and heated at 95 °C for 3 min. Reaction products were analyzed on 20% denaturing polyacrylamide gels. Gels were visualized by phosphorimaging analysis (Typhoon FLA 9000, GE Healthcare, Europe).

Ligand degradation under oxidative conditions

The formation of ligand degradation products under oxidative conditions was monitored for 2h recording HPLC chromatograms each 15 mins (analytical method).
A NDI-Cu-DETA stock solution (1.041 mM in water) was diluted in 50 mM phosphate buffer, at pH 7.4 until a final concentration of 6.25 μM or 12.5 μM and left at 37 °C for 3 hrs. A solution of KCl (100 mM) was added to mimic the DNA cleavage conditions. The first profile was registered after 2.5 mins from H_2O_2 (1 mM) and ascorbate (1 mM) addition in the solution. The same experiment was conducted in the presence of LTR-III, previously folded into G4 structure.

A stock solution of LTR-III (50 μM) was prepared in 10 mM Tris buffer at pH 7.4 in presence of KCl salt (100 mM), then the NA were annealed by incubation at 95 °C for 5 mins and subsequently cooled down at room temperature overnight. The folded sample (12.5 μM) was incubated with NDI-Cu-DETA complex (6.25 μM) for 24 h at room temperature before starting the oxidative experiment as reported before.

To identify the chemical structure of the ligand degradation products, the oxidative reaction was performed with a large amount of NDI-Cu-DETA (20 mg) in 50 mM phosphate buffer at pH 7.4, and the derivatives were purified by HPLC and characterized by MS direct injection and NMR.

DEG-1: orange solid (Analytical method: t_R= 6.27 min), MS direct injection in methanol (DEG-1-H^+: 410 m/z, DEG-1-H_2^{2+}:206 m/z), ^{1}H-NMR (300 MHz, CD_3OD): δ (ppm) = 8.38 (bs, 1H); 8.16 (bs, 1H); 7.86 (s, 1H); 4.52 (bs, 4H); 3.55 (bs, 2H); 3.42 (bs, 2H); 3.06 (s, 6H); 2.79 (s, 3H).

DEG-2: orange solid (Analytical method: t_R= 6.40 min), MS direct injection in methanol (424 DEG-2-H^+:424 m/z, DEG-2-H_2^{2+}: 213 m/z), ^{1}H-NMR (300 MHz, CD_3OD): δ (ppm) = 8.64-8.62 (m, 1H); 8.37-8.34 (m, 1H); 8.22 (s, 1H); 4.6-4.56 (m, 4H); 3.59 (bs, 4H); 3.06 (s, 12H). ^{13}C NMR (75 MHz, CD_3OD) δ 167.5, 165.6, 164.9, 155.2, 132.2, 131.5, 129.3, 127.9, 127.0, 125.6, 125.1, 121.8, 100.4, 57.9, 57.5, 44.5, 44.4, 37.1, 36.7.

MS analysis. Bands of interest were excised from denaturing polyacrylamide gels (see DNA selective cleavage), cut into small pieces and extracted in water overnight. Desalting of the extracted cleavage products was performed by ultrafiltration against HFIP/TEA pH 7.4 (150 mM hexafluoroisopropanol, pH adjusted to 7.4 with triethylamine) in Millipore (North Bend, OH, USA) Amicon Ultra devices with 3 kDa MWCO. The samples were added with 20% isopropanol and analyzed by direct infusion electrospray ionization (ESI). Digestion with Nuclease S1 (Fermentas) was performed using 30 units of enzyme for 30 minutes at 37 °C in 100 mM ammonium acetate pH 4.6. For stoichiometric and binding affinities calculation oligonucleotides were heat-denatured in 0.8 mM KCl, HFIP/TEA pH 7.4. The samples were folded by letting cool to room temperature in 2 hours and adding 20% of isopropanol (IPA) before incubating overnight at 4 °C. The oligonucleotides were diluted to final concentration of 5 μM and incubated with the tested compounds at 1:2 ratio DNA:compound overnight at 4 °C. The reconstructed-ion chromatogram area for each species calculated by MassLynx V4.1 was insert in the following formula: [BA = (ΣG4b/(ΣG4f + ΣG4b)) × 100] to calculate the binding affinity of NDI-Cu-DETA to the tested G4. BA is the binding affinity, G4b is chromatogram area of bound G4 DNA, and G4f is the chromatogram area of free G4 DNA. [S6] The ESI-MS spectra were recorded using a Xevo G2-XS QTof mass spectrometer (Waters, Manchester, UK). The injection of the samples to the Xevo mass spectrometer was automatically performed by an Agilent 1290 Infinity HPLC (Agilent

Technologies, Santa Clara, CA, US) equipped with an auto sampler; the carrying buffer was HFIP adjusted to pH 7.4 with TEA and supplied with 20% of isopropanol. The electrospray capillary was set at 1.8 kV, the source and desolvation temperatures were 45 and 65 °C, respectively, and the sampling cone was at 65 V. The collision energy was set at 20-25 V during tandem mass spectrometry (MS/MS) experiments.

NMR titration. NMR titration was carried out using Bruker Avance II 600 MHz and Avance III 800 MHz machines at 25ºC. Oligonucleotide concentrations for LTR-III, c-myc, and c-kit1 were 100 µM, with buffer containing 70 mM KCl, 20 mM KPi, and 10% D_2O at pH 7.0. Addition of NDI-Cu-DETA was done from stock solution of 10 mM to desired concentrations, with the corresponding NMR spectra recorded immediately after addition. All NMR spectra were processed and analyzed using Bruker TopSpin 2.1.

Molecular modelling. MGL tools 1.5.6 with AutoGrid4 and AutoDock Vina were used to set up and exert blind docking calculations between Cu-DETA and the DNA sequence LTR-III.[S7] The geometries of the ligands were optimized prior to the docking studies: the solubilizing chains on the NDI were first replaced by methyl groups and the ligand was geometry optimized by DFT calculations refined at B3LYP/6-311+G** level of theory by using Gaussian09 (see Gaussian Output); the solubilizing chains were appended and geometry optimized by using Spartan08 keeping the core structure frozen, according to a double protonated species at pH = 7.0 (Table S1). DNA and ligand files were provided using AutoDock Tools. The DNA was enclosed in a box with number of grid points in x_y_z directions, 42_32_40 and an exhaustiveness of 536. Lamarckian genetic algorithms, as accomplished in AutoDock Vina, were employed to perform docking calculations. All other parameters were default settings. Visualization of the docked pose has been carried out by using UCSF Chimera molecular graphics program.

Supplementary Figures, Table and Data:

Metallo-Complex Characterization:

1-Potentiometric and pH-spectrophotometric titration in water.

Potentiometric and pH-spectrophotometric experiments were typically performed by addition of standard NaOH to a solution of **NDI-DETA** in the fully protonated form. Titrations were run in both the absence and presence of 1 eqv. Cu(II).

A) B)

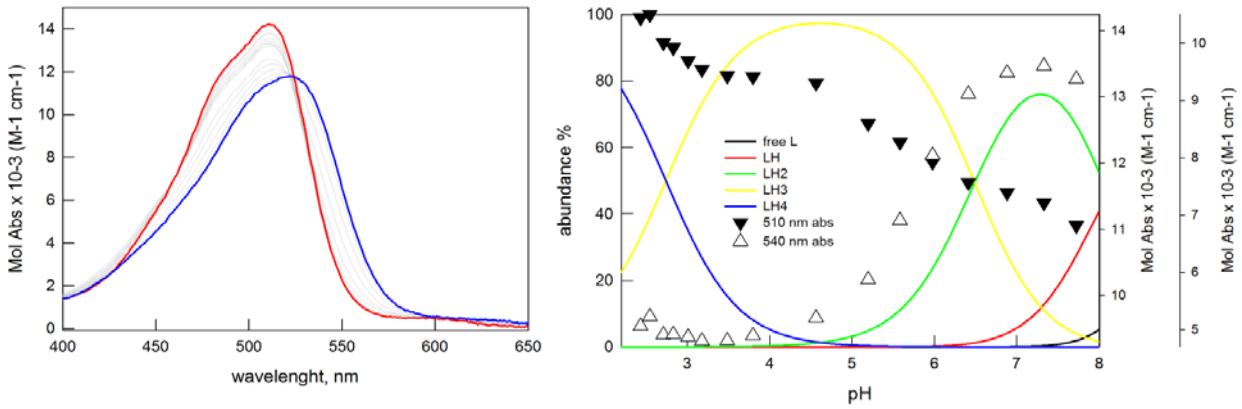

Figure S1. A) Family of UV-vis. spectra taken upon pH-spectrophotometric titration of **NDI-DETA** (0.09 mM, T=25°C) in 0.1M $NaNO_3$. Red line: spectrum at pH=2; blue line: final spectrum taken at pH 8. B) Speciation analysis resulting from the potentiometric titration for **NDI-DETA.** Lines: distribution diagram of the species as % abundance vs. pH. Black and white triangles describe the absorption changes monitored at 510 nm and 540 nm, respectively. The corresponding constants are shown in Table S1 A).

Experimental results were fitted using the HyperQuad package;[S8] the resulting protonation constants are reported in Table S1A). From the potentiometric experiment on the free ligand, four protonation constants could be determined. In particular, **[NDI-DETAH]$^{+}$**, **[NDI-DETAH$_2$]$^{2+}$**, **[NDI-DETAH$_3$]$^{3+}$** and **[NDI-DETAH$_4$]$^{4+}$** species were observed to form under protonation of the tertiary amino groups. The fully protonated species [NDI-DETAH$_4$]$^{4+}$ displays an absorption band at 512 nm (3500 M^{-1} cm^{-1}), typical of the NDI unit (see the red line in Figure S1). Upon deprotonation, this band decreases in intensity and undergoes a red shift. At pH ≥ 8, the color in solution turns from orange to yellow, following NDI decomposition. No deprotonation of the N-H groups conjugated to the NDI unit was observed.

In the presence of Cu(II) [i.e. 1 eqv. of Cu(ClO_4)$_2$], the color change observed in the 4 < pH < 8 interval, from orange to violet, as well as the red-shift (about 100 nm) of the absorption band are attributed to complexation. Over pH 6, only Cu(II)-containing species are present in solution. In particular, at physiological pH values, the dominant species are **[NDI-Cu-DETAH]$^{2+}$** and **[NDI-Cu-DETA]$^{+}$**. In basic conditions, the deprotonation of a water molecule bound to the Cu(II) center leads to the formation of **[NDI-Cu(OH)-DETA]**. Differently from the free ligand case, no decomposition of the NDI unit is observed. Equilibria were investigated by potentiometric studies and the corresponding constants are shown in Table S1B.

Table S1: A) Protonation and B) Cu(II) complexation constants for **NDI-DETA** in Log units (standard deviations in parentheses)

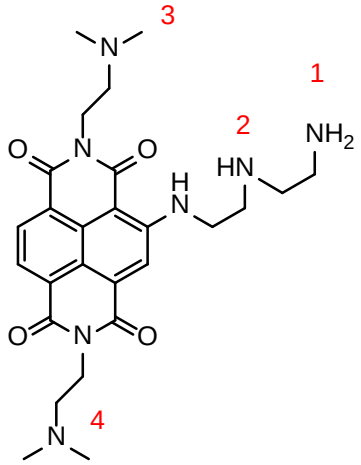

A)

	Log β values
[**NDI-DETA**H]$^{+}$	8.90(1)
[**NDI-DETA**H$_2$]$^{2+}$	17.01(1)
[**NDI-DETA**H$_3$]$^{3+}$	23.50(1)
[**NDI-DETA**H$_4$]$^{4+}$	26.22(2)

B)

	Log β values
[**NDI-Cu-DETA**H$_2$]$^{3+}$	30.13(1)
[**NDI-Cu-DETA**H]$^{2+}$	25.56(2)
[**NDI-Cu-DETA**]$^{+}$	17.87(2)
[**NDI-Cu(OH)-DETA**]	10.63(2)

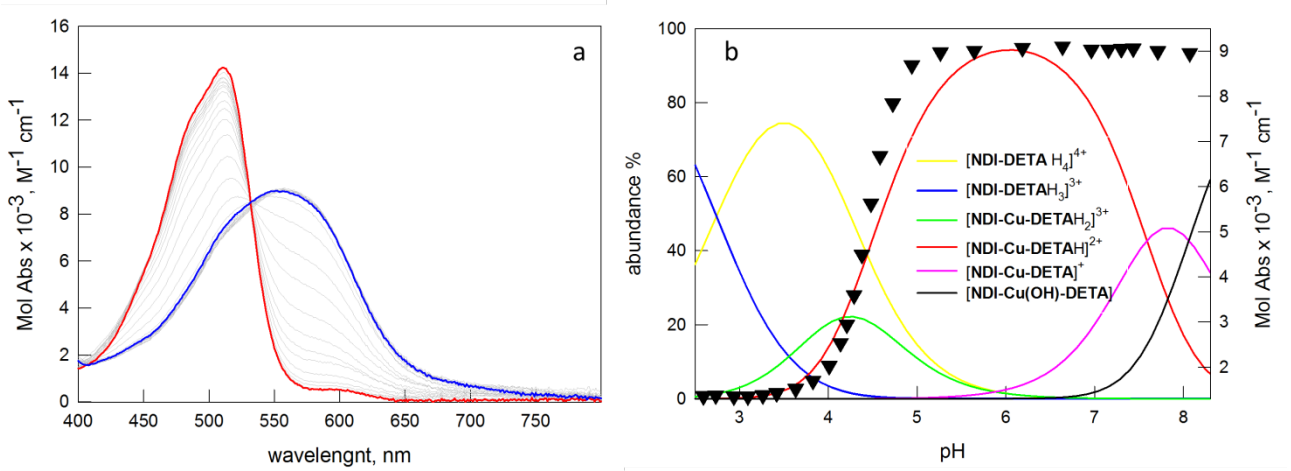

Figure S2. A) UV-vis. spectra taken upon pH-spectrophotometric titration of **NDI-DETA** (0.09 mM), in the presence of 1 eqv. $Cu(ClO_4)_2$ (0.1 M $NaNO_3$, at 25°C). Red line = initial spectrum at pH 2.5; blue line = spectrum at pH 8.2. B) Distribution diagram of the species (% abundance vs. pH) obtained upon potentiometric titration of **NDI-DETA** (0.09 mM), in the presence of 1 equiv. $Cu(ClO_4)_2$ (0.1 M at 25 °C). The corresponding constants are shown in Table S1 B). Black triangles: profile of Mol Abs ($\times 10^{-3}$, M^{-1} cm^{-1}) at 557 nm vs. pH.

In the fully protonated form, **[NDI-DETAH$_4$]$^{4+}$**, the ligand ($9 \cdot 10^{-6}$ M) displays an emission band at 565 nm typical of the NDI unit (λ_{exc} = 524 nm, i.e. isosbestic point in the pH-spectrophotometric titration). The fluorescence quenching observed upon addition of NaOH(aq) was attributed to the photoinduced electron transfer (PET) from the deprotonated tertiary amines to NDI.[S9] Notably, in the presence of Cu(II), the emission intensity of the ligand is very low even in acidic conditions, probably due to the heavy atom effect, thus the corresponding pH-spectrofluorimetric titration was not performed.

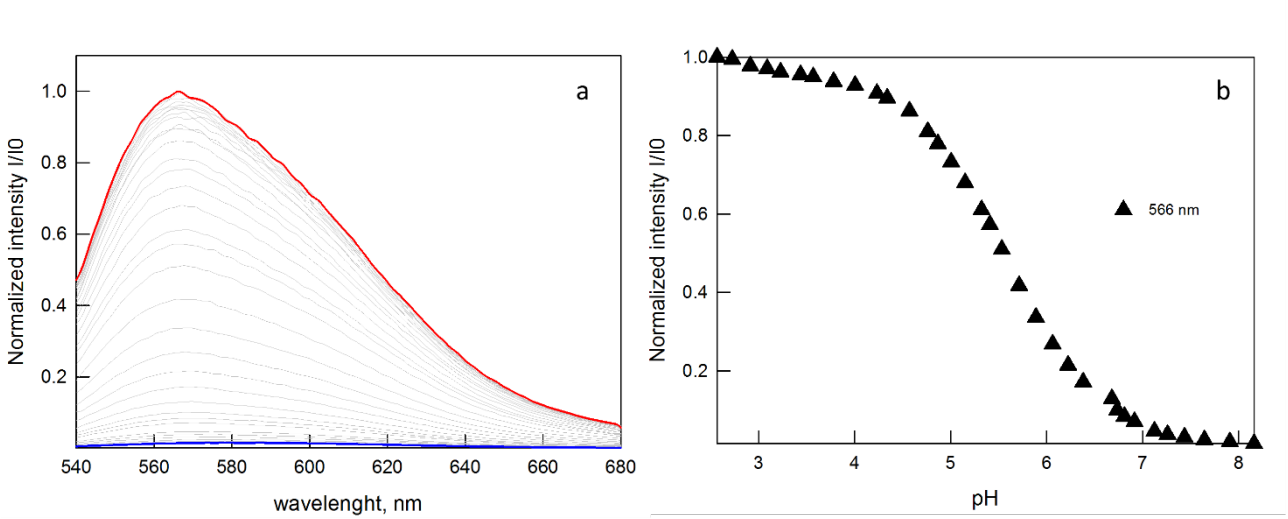

Figure S3. A) Family of emission spectra recorded over the pH-spectrophotometric titration of **NDI-DETA** (9 μM, T=25 °C, 0.1 M $NaNO_3$). Red line: initial spectrum at pH=2.5; blue line: spectrum at pH=8. B) Profile of the normalized intensity at 500 nm vs. pH, corresponding to the pH-spectrofluorimetric titration of **NDI-DETA** (9 μM) (λ_{exc} = 524 nm).

2-Spectrophotometric titration with metal ions in aqueous solution (pH=7).

The UV-vis titration of **NDI-DETA** with Cu(II) in aqueous solution at pH=7 (HEPES 0.1 M, 25 °C) confirmed the outstanding affinity of the ligand for copper, and the formation of a 1:1 complex.

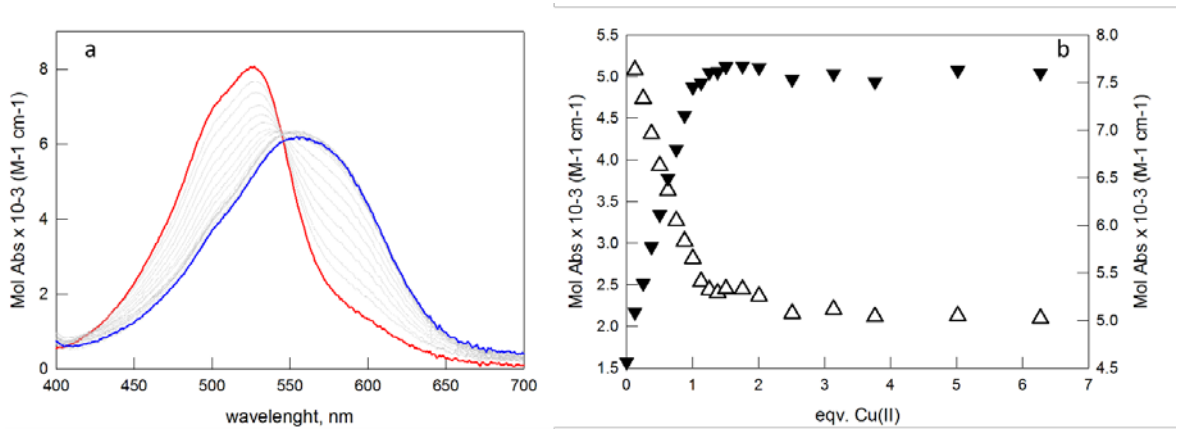

Figure S4. A) Spectrophotometric titration of **NDI-DETA** (0.02 mM) with $Cu(ClO_4)_2$ (0.4 mM) in 0.1 M HEPES pH=7 (l=10 cm) (path length=10 cm). B) Titration profiles obtained at 524 nm (black triangles) and 590 nm (white triangles).

Upon addition of Cu(II), the initial absorption band (red line in Fig. S4A), attributable to the NDI unit of the ligand, decreased in intensity and shifted towards lower energies. The final spectrum corresponds to the blue line in Fig. S4A. This remarkable shift is due to the deprotonation of the N–H bond conjugated to the NDI core upon copper binding. A similar shift was observed in our previous studies [S9] on another polyamino-ligand containing a NDI core. Unfortunately, the titration curve was too steep for a safe calculation of the binding constant (see Fig. S4B).

Titration experiments were also carried out with other transition metal ions, M(II) (Co, Ni, Zn, Hg). As shown by the plots of the normalized absorbance (A/A_0) at 524 nm vs. equivalents of the added M(II) (Fig. S5), the affinity of **NDI-DETA** for Cu(II) is definitely higher than for all the other investigated metal species.

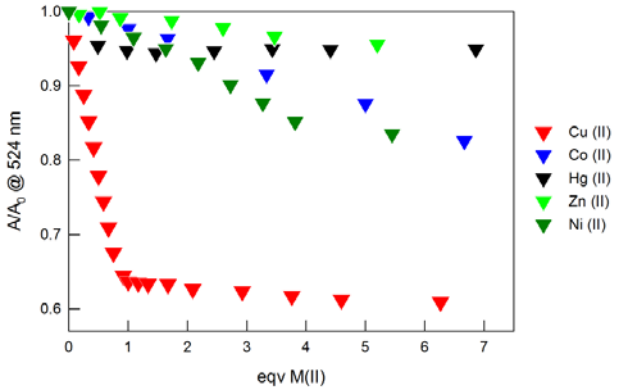

Figure S5. UV-vis. profiles of A/A_0 @ 524 nm for **2**·4HCl (0.06 mM) vs. mM concentration of the chosen transition metal ion [M(II) : Cu(II), Ni(II), Co(II), Zn(II) and Hg(II)] in 0.1 M HEPES pH 7 (T=25 °C).

However, in the case of Ni(II) and Co(II), the equilibrium constants for the formation of 1:1 complexes could be determined [Log K_{11} = 3.4(2) and 2.87 (1) for Ni(II) and Co(II), respectively]. The corresponding distribution diagrams are shown in Fig. S6.

The Cu(II) binding constant was obtained by a competition titration experiment, using **Tren** (i.e. N,N,N-triethylentetramine) as the competing ligand. In particular, this ligand is known to form a stable 1:1 complex with Cu(II) in water, with a binding constant as high as 18.8 Log units. [S10] In the competition experiment, we performed the UV-vis. titration of a solution of the in-situ prepared **NDI-Cu-DETA** complex (50 μM in 0.1M HEPES, pH 7) with a solution of **Tren**. As expected, the competing ligand displaced Cu(II) from the **NDI-Cu-DETA** complex and thus promoted the recovery of the absorption band of the free **NDI-DETA.**

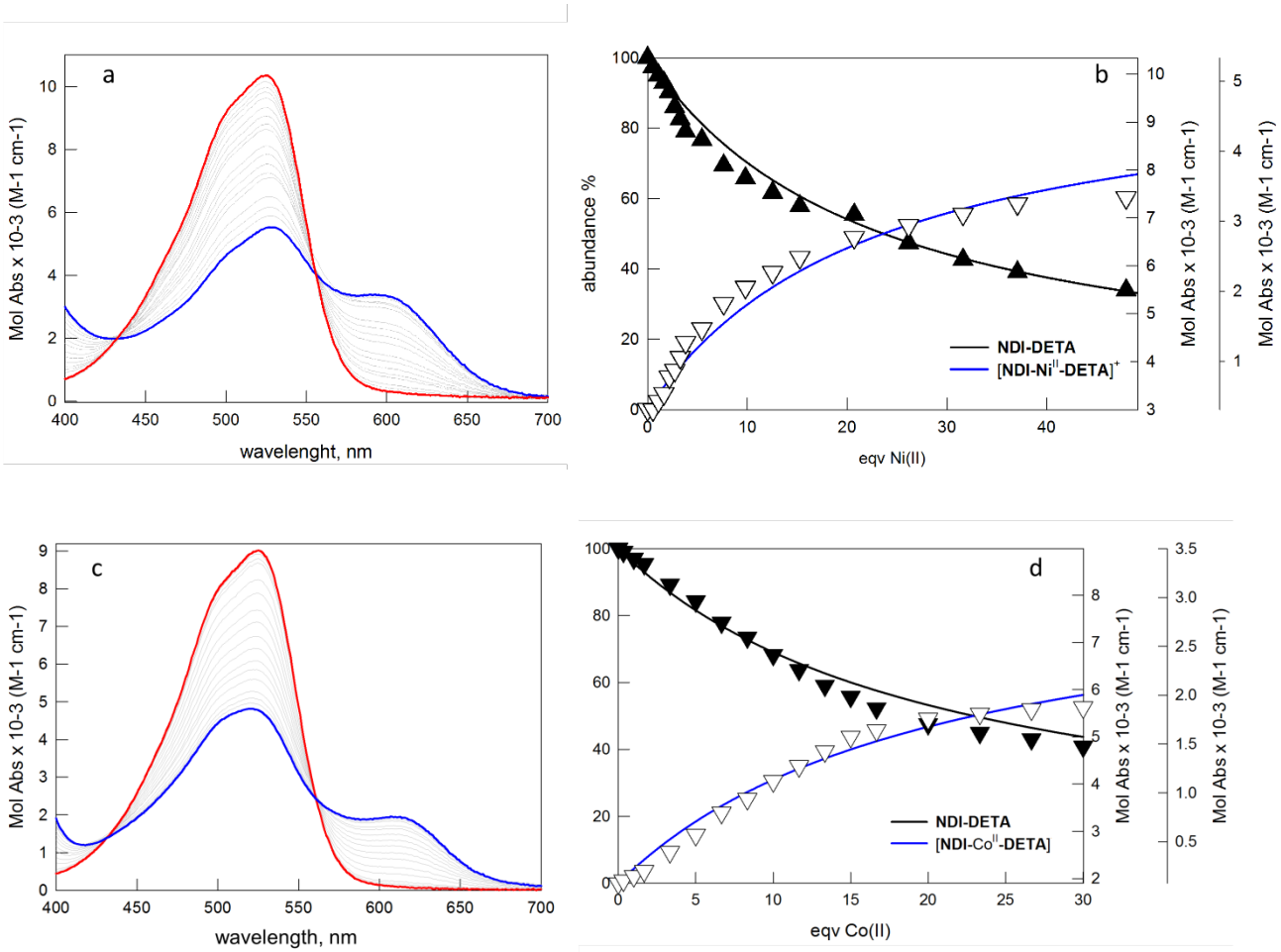

Figure S6. Spectrophotometric titration of **NDI-DETA** (0.06 mM) with $Ni^{II}(CF_3SO_3)_2$ A) and $Co^{II}(CF_3SO_3)_2$ C) in 0.1 M HEPES pH=7. Red line: initial spectrum of the free ligand; blue line: final spectrum with an excess of M(II). B) and D): Distribution diagrams of the species for the titrations with Ni(II) and Co(II), respectively. Black triangles: profile of Mol Abs ($\times 10^{-3}$, M^{-1} cm^{-1}) at 524 nm; white triangles: profile of Mol Abs ($\times 10^{-3}$, M^{-1} cm^{-1}) at 600 nm.

Table S2. Oligonucleotides used in this study

Assay	Name	Sequence 5'-3'
FRET	hTel	*FAM*-GGGTTAGGGTTAGGGTTAGGG-*TAMRA*
	c-myc	*FAM*-TGGGGAGGGTGGGGAGGGTGGGGAAGG-*TAMRA*
	bcl-2	*FAM*-AGGGGCGGGCGCGGGAGGAAGGGGGCGGGAGCGGGGCTG-*TAMRA*
	c-kit 1	*FAM*-AGGGAGGGCGCTGGGAGGAGGG-*TAMRA*
	c-kit 2	*FAM*-CGGGCGGGCGCGAGGGAGGGG -*TAMRA*
	LTR-III	*FAM*-GGGAGGCGTGGCCTGGGCGGGACTGGGG-*TAMRA*
	LTR-IV	*FAM*-TGGGCGGGACTGGGGAGTGGT-*TAMRA*
	LTR-III+IV	*FAM*-TGGGAGGCGTGGCCTGGGCGGGACTGGGGAGTGGT-*TAMRA*
	ds DNA	*FAM*-CAATCGGATCGAATTCGATCCGATTG-*TAMRA*
CD/DNA cleavage	hTel22	AGGGTTAGGGTTAGGGTTAGGG
	ss scrambled hTel22	GGATGTGAGTGTGAGTGTGAGG
	ss compl. scrambled hTel22	CCTCACACTCACACTCACATCC
	ds scrambled hTel22	ss scrambled hTel22 + ss compl. scrambled hTel22
	c-myc	TGAGGGTGGTGAGGGTGGGGAAGG
	bcl-2	GGGCGCGGGAGGAAGGGGGCGGG
	c-kit 1	AGGGAGGGCGCTGGGAGGAGGG
	c-kit 2	CGGGCGGGCGCGAGGGAGGGG
	LTR-III	GGGAGGCGTGGCCTGGGCGGGACTGGGG
	ss mut LTR-III	GTGATGCGTGTCCTGTGCGTGACTTGTG
	ss mut compl. LTR-III	CACAAGTCACGCACAGGACACGCATCAC
	ds mut LTR-III	ss mut LTR-III + ss mut compl. LTR-III
	LTR-III+IV	TGGGAGGCGTGGCCTGGGCGGGACTGGGGAGTGGT
	LTR-IV	TGGGCGGGACTGGGGAGTGGT
	un2	GGGGGCGAGGGGCGGGAGGGGGCGAGGGG
	ss mut un2	GTGTGCGAGTGTCGTGAGTGTGCGAGTGT
	ss mut compl. un2	ACACTCGCACACTCACGACACTCGCACAC
	ds mut un2	ss mut un2 + ss mut compl. un2
	un3	GGGAGGAGCGGGGGGAGGAGCGGG
	gp054b	GGGGTTGGGGTTGGGGTTGGGG
	ss mut gp054b	TGTGTTGTGTTTGTGTTTGTGT
	ss mut compl. gp054b	ACACAAACACAAACACAACACA
	ds mut gp054b	ss mut gp054b + ss mut compl. gp054b
	gp054e	GGGGCTGGGGCTGGGGTTGGGG

Table S3. FRET analysis of **NDI-Cu-DETA** and **NDI-DETA** binding towards G4s and control sequences. T_m and ΔT_m values (°C) measured by FRET melting in the presence of 0.25 µM oligonucleotides, 1 µM compound, in 10 mM lithium cacodylate buffer, at increasing K^+ concentrations (20, 50, 100 mM). NA stands for Nucleic Acid sequence.

NA	*K^+ 20 mM*					*K^+ 50 mM*					*K^+ 100 mM*				
	T_m	**NDI-Cu-DETA** T_m	ΔT_m	**NDI-DETA** T_m	ΔT_m	T_m	**NDI-Cu-DETA** T_m	ΔT_m	**NDI-DETA** T_m	ΔT_m	T_m	**NDI-Cu-DETA** T_m	ΔT_m	**NDI-DETA** T_m	ΔT_m
hTel	51.9 ± 0.1	72.6 ± 0.5	20.7	75.9 ± 0.1	24.0	58.9 ± 0.1	74.6 ± 0.6	15.7	77.2 ± 0.5	18.3	63.9 ± 0.1	76.6 ± 0.6	12.7	78.9 ± 0.8	15.0
dsDNA	55.9 ± 0.1	58.9 ± 0.1	3.0	60.6 ± 0.5	4.7	58.9 ± 0.1	60.6 ± 0.5	1.7	59.9 ± 0.1	1.0	59.9 ± 0.1	60.9 ± 0.1	1.0	61.9 ± 0.1	2.0
c-myc	>90	>90	ND	>90	ND	>90	>90	ND	>90	ND	>90	>90	ND	>90	ND
bcl-2	>90	>90	ND	>90	ND	>90	>90	ND	>90	ND	>90	>90	ND	>90	ND
c-kit1	47.3 ± 0.5	59.3 ± 0.6	12.0	60.6 ± 0.6	13.3	52.9 ± 0.1	61.9 ± 0.1	9.0	64.9 ± 0.5	12.0	57.9 ± 0.1	65.9 ± 0.1	8.0	68.2 ± 0.5	10.3
c-kit2	56.3 ± 0.6	73.9 ± 0.1	17.6	76.6 ± 0.5	20.3	63.4 ± 0.9	75.2 ± 0.6	11.8	77.9 ± 0.1	14.5	71.6 ± 0.8	77.2 ± 0.6	5.6	78.9 ± 0.1	7.3
LTR-III	49.0 ± 0.1	65.9 ± 0.1	16.9	68.2 ± 0.5	19.2	54.3 ± 0.5	68.2 ± 0.4	13.9	70.9 ±0.1	16.6	59.9 ± 0.1	71.2 ± 0.5	11.3	72.9 ± 0.1	13.0
LTR-IV	42.0 ± 0.1	60.9 ± 0.1	18.9	66.2 ± 0.5	24.2	45.9 ± 0.1	66.2 ± 0.5	20.3	70.9 ± 0.1	25.0	50.6 ± 0.4	67.9 ± 0.3	17.3	70.9 ± 0.1	20.3
LTR-III+IV	51.9 ±0.1	72.6 ± 0.5	20.7	75.9 ± 0.1	24.0	58.9 ± 0.1	74.6 ± 0.6	15.7	77.2 ± 0.5	18.3	63.9 ± 0.1	76.6 ± 0.6	12.7	78.9 ± 0.8	15.0

Table S4. CD analysis of **NDI-Cu-DETA** binding towards G4 sequences. ΔT_m values measured by CD melting of 4 µM oligonucleotides, in the presence of 16 µM compound, in 10 mM lithium cacodilate buffer, at the indicated K^+ concentrations.

Sequence name	**Organism**	**G4 prevalent topology**	**Wavelength**[§]	**K^+conc.** (mM)	**T_m** (°C)	**NDI-Cu-DETA T_m** (°C)	**ΔT_m** (°C)
hTel22	mammalian	Hybrid[S11]	264 nm	20	59.4 ± 0.6	83.0 ± 0.3	23.6
c-myc	mammalian	Parallel[S12]	265 nm	5	54.8 ± 0.1	88.1 ± 0.7	33.3
bcl-2	mammalian	Parallel[S13]	265 nm	5	59.7 ± 0.5	87.2 ± 0.2	27.5
c-kit1	mammalian	Parallel[S14]	265 nm	50	58.7 ± 0.2	76.1 ± 0.6	17.4
c-kit2	mammalian	Parallel[S15]	265 nm	20	60.9 ± 0.1	>90	>29.1
LTR-III	HIV-1	Hybrid[S7, S16]	265 nm	10	55.2 ± 0.2	76.2 ± 0.6	21.0
LTR-IV	HIV-1	Parallel[S17]	265 nm	100	50.4 ± 0.4	73.3 ± 0.4	22.9
LTR-III+IV	HIV-1	Hybrid[S7]	265 nm	150	56.6 ± 0.3	81.9 ± 0.9	25.3
un2	HSV-1	Antiparallel[S18]	295 nm	0.05	59.3 ± 0.4	64.0 ± 0.6	4.7
un3	HSV-1	Parallel[S18]	265 nm	20	53.5 ± 0.9	63.8 ± 0.8	10.3
gp054b	HSV-1	Hybrid[S18]	264 nm	2	56.7 ± 0.3	85.7 ± 0.4	29.0
gp054e	HSV-1	Hybrid[S18]	264 nm	2	56.7 ± 0.3	78.6 ± 0.9	21.9

*G4 prevalent topology, as assessed by CD analysis.

§ Wavelength used to monitor CD melting.

Catalytic oxidation of 4-tert-butylcatechol.

NDI-Cu-DETA capacity to involve oxidative modifications on biological substrates, exploiting the copper redox activity, has enormous relevance in this context. We therefore followed the oxidation of 4-tert-butylcatechol (4TBC) whose product of oxidation is 4-tert-butylquinone that presents a characteristic band at 400 nm (ε_{400nm} = 1210 $cm^{-1}M^{-1}$).[S3]

We compared the profile obtained with NDI-Cu-DETA, previously complexed, with copper free and with NDI-DETA where the copper ion is added directly in reaction environment (Figure S8).

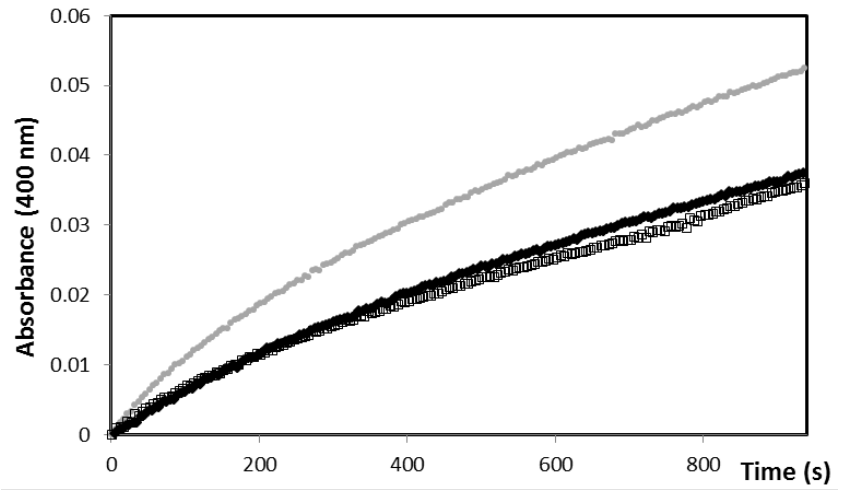

Figure S7. Kinetics profile of 4TBC (3 mM) oxidation with time in the presence of Cu^{2+} (25 µM) (grey dots), of NDI-Cu-DETA complex (25 µM) (black diamonds) and of Cu^{2+} (25 µM) with NDI-DETA ligand (25 µM) (empty squares) in 50 mM phosphate buffer solution at pH 7.4 and 25°C.

NDI-Cu-DETA presents a slightly lower kinetic trend (v_i = 2.6 ms^{-1}) to that of free copper (v_i = 3.8 ms^{-1}), that may depend on the difficulty of the substrate to interface with the binder for steric hindrance.

Interesting is the profile obtained with the addition in solution of NDI-DETA and Cu^{2+} not previously complexed, that results almost identical to that of NDI-Cu-DETA complex. These results allow us to suppose that the copper ion remains coordinated to the NDI-DETA ligand under the turnover conditions, in addition to confirming the high binding affinity between NDI-DETA and copper ion.

Characterization of reactive oxygen species involved.

Different experiments were carried out to identify specific ROS that might contribute in the DNA cleavage reaction promoted by ascorbic acid/NDI-Cu-DETA/H_2O_2 system. Actually, this system involves copper in low oxidation state that can catalyse decomposition of hydrogen peroxide via the Fenton reaction, which yields hydroxyl radicals (˙OH):[S19]

$Cu^{+} + H_2O_2 \rightarrow Cu^{2+} + {}^{\cdot}OH + OH^{-}$

Hydroxyl radical is a short-lived radical which can subsequently reacts with DNA at nearly diffusion-controlled rates[S20] and causes serious lesions to them.[S21]

Besides, it was proposed that neither $O_2^{\cdot -}$ nor H_2O_2 at physiological concentrations causes any strand breakage or chemical modification of the nucleic bases.[S22] Nevertheless, their interaction with transition-metal ions forms hydroxyl radicals (˙OH) that could damage the DNA in cells.

To confirm the involvement of the hydroxyl radicals, already sensed from the complete DNA cleavage inhibition by catalase, the bleaching of *p*-nitroso-N,N-dimethylaniline (p-NDA) was

used.[S4, S23] In fact, the chromophore-NO group of p-NDA was bleached to a colourless -NO_2 group specifically by ˙OH with an estimated rate constant around 10^{10} $M^{-1}s^{-1}$.[S4]

The bleaching of p-NDA in the presence of H_2O_2 and ascorbate was spectrophotometrically monitored at 440 nm in 10 mM Tris-HCl buffer (pH 7.4) at 37 °C, after the addition of NDI-Cu-DETA complex (black trace in Figure S8) or of NDI-Cu-DETA previously bound to c-myc or LTR-III oligomers fold into G4 structure (green and red trace respectively in Figure S8A).

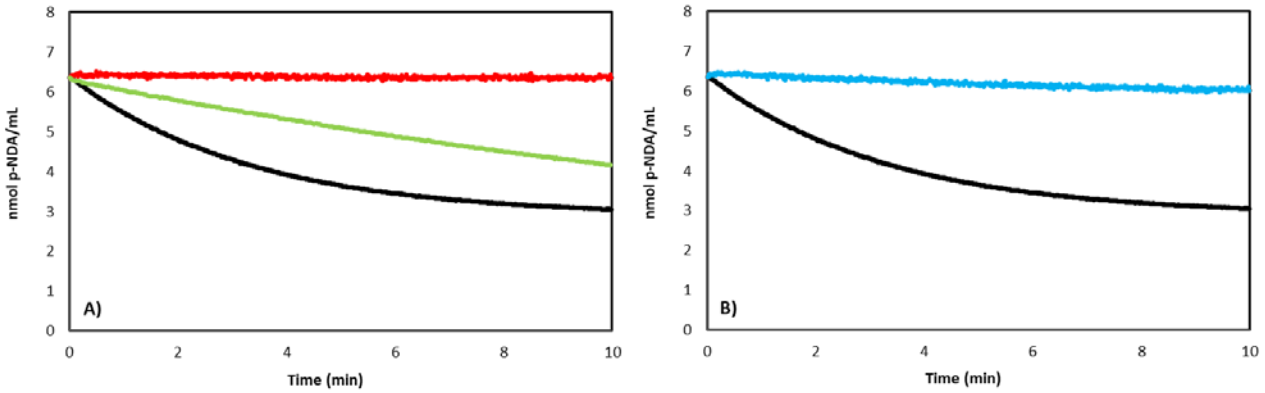

Figure S8. Hydroxyl radical-mediated decreasing of p-NDA absorbance at 440 nm in 10 mM Tris-HCl buffer (pH 7.4) at 37 °C in presence of p-NDA (6.25 µM), H_2O_2 (1 mM), ascorbate (1 mM) and with the addition of **A)** NDI-Cu-DETA (6.25 µM) complex (black trace); NDI-Cu-DETA (6.25 µM) complex previously incubated with c-myc (12.5 µM) in G4 structure (green trace) or LTR-III (12.5 µM) in G4 structure (red trace); **B)** NDI-Cu-DETA (6.25 µM) complex (black trace) or NDI-Cu-DETA (6.25 µM) complex in the presence of mannitol (0.625 mM) (blue trace).

As it is possible to note from Figure S8A, without DNA the p-NDA bleaching reaches the saturation after around 6 min in the reaction conditions used, confirming the formation and the involvement of diffusible hydroxyl radical. On the contrary, the ligand interaction with G4s makes the oxidation of the nucleic bases a competitive process, decreasing the formation of *p*-nitrodimethylaniline. In particular, the presence of LTR-III-G4 completely inhibits the reaction of hydroxyl radical with p-NDA.

As it is possible to note from Figure S8B, the addition of 100 equiv. of mannitol inhibits the ˙OH-dependent bleaching of p-NDA, without G4s presence, confirming its role as hydroxyl radical scavenger.

The addition of H_2O_2 alone,[S4] such as ascorbate alone, or NDI-Cu-DETA alone could not induce the decreasing of p-NDA absorbance (data not show).

These results rule out the possibility of DNA cleavage by hydroxyl radicals.

NDI-Cu-DETA cleavage on mutant ssDNA and dsDNA sequences derived from LTR-III, un2 and gp054b.

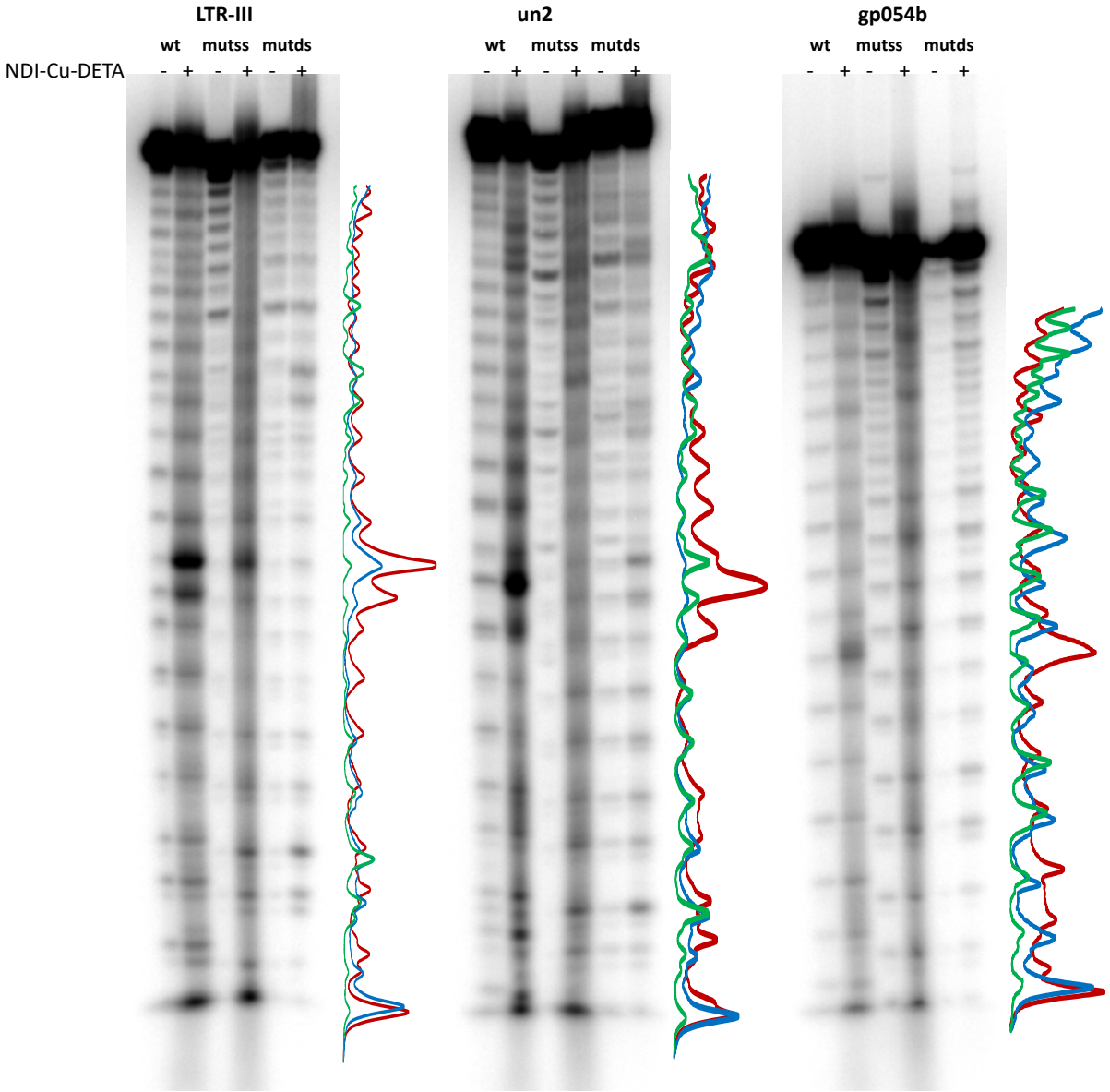

Figure S9. NDI-Cu-DETA-induced cleavage of wild type G4-folded sequences (LTR-III, un2, gp054b), mutated sequences derived from them (mut ss) and their dsDNA (mut ds) (Table S2). Oligonucleotides (0.25 µM) were reacted with **NDI-Cu-DETA** (3.12 µM) for 2.5 min in the presence of 1 mM sodium ascorbate and 1 mM hydrogen peroxide. Samples were run on denaturing polyacrylamide gels. Panels include intensity profiles of wtDNA (red lines), mutant ssDNA (blue lines) and mutant dsDNA (green lines).

NDI-Cu-DETA cleavage on LTR-III, un2 and gp054b, in the presence of ds DNA competitor.

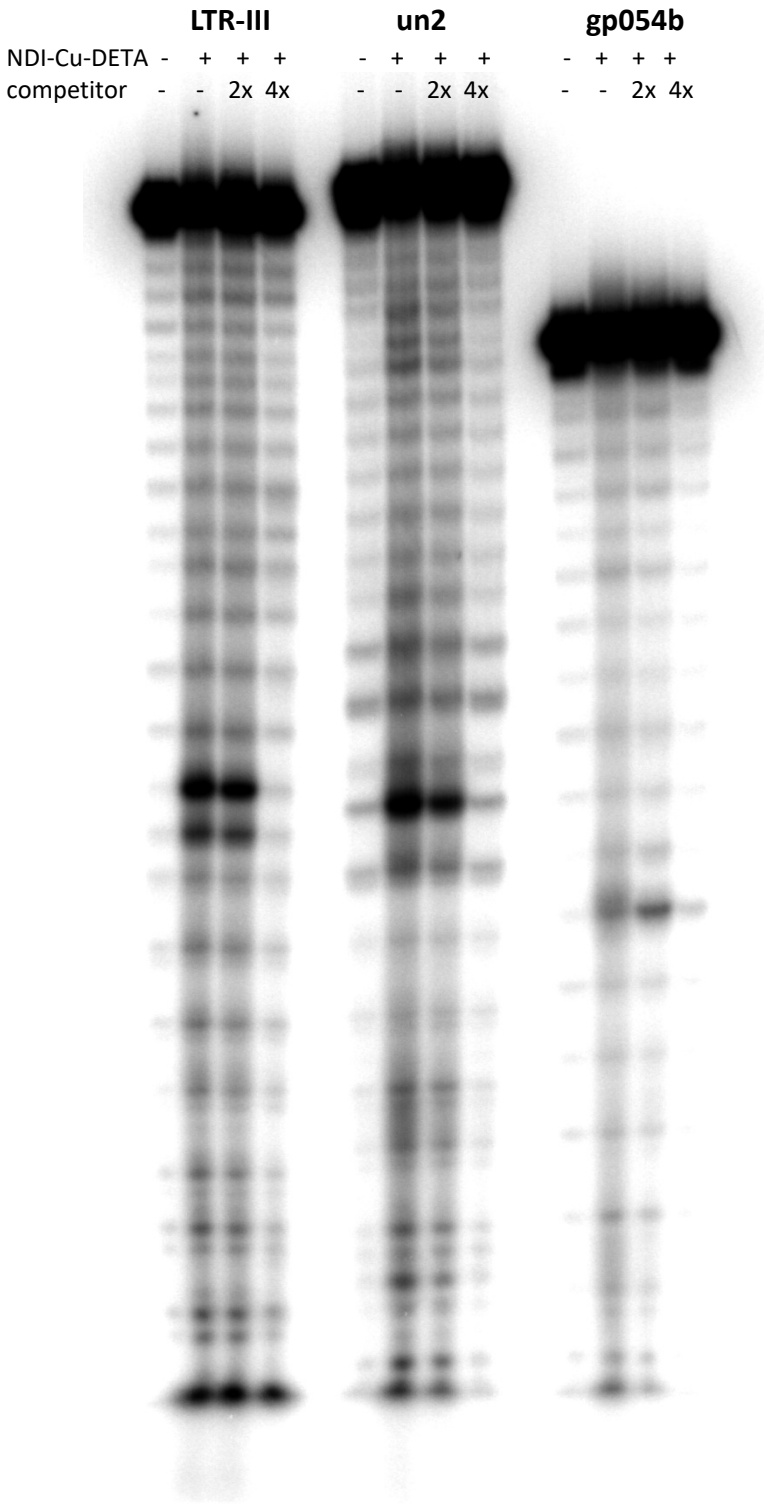

Figure S10. NDI-Cu-DETA-induced cleavage of wild type G4-folded sequences (LTR-III, un2, gp054b) in the presence of 2- and 4-folds of dsDNA competitor. Competitor sequences are ds mutant sequences derived from the wt oligonucleotides (Table S2). Oligonucleotides (0.25 µM) were reacted with **NDI-Cu-DETA** (3.12 µM) for 2.5 min in the presence of 1 mM sodium ascorbate and 1 mM hydrogen peroxide. Samples were run on denaturing polyacrylamide gels.

NDI-Cu-DETA cleavage on c-myc, bcl-2, c-kit1 and c-kit2 G4s.

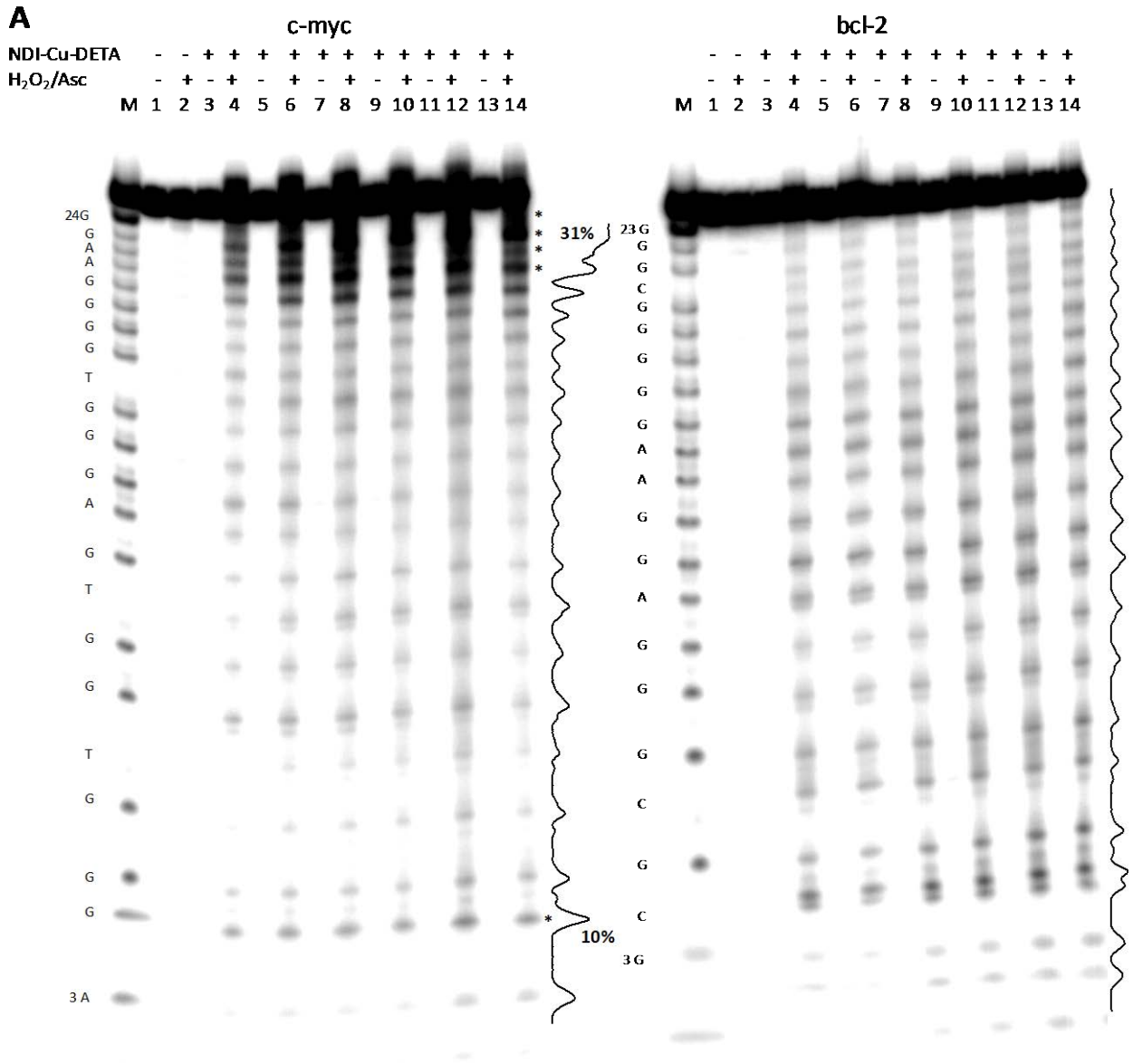

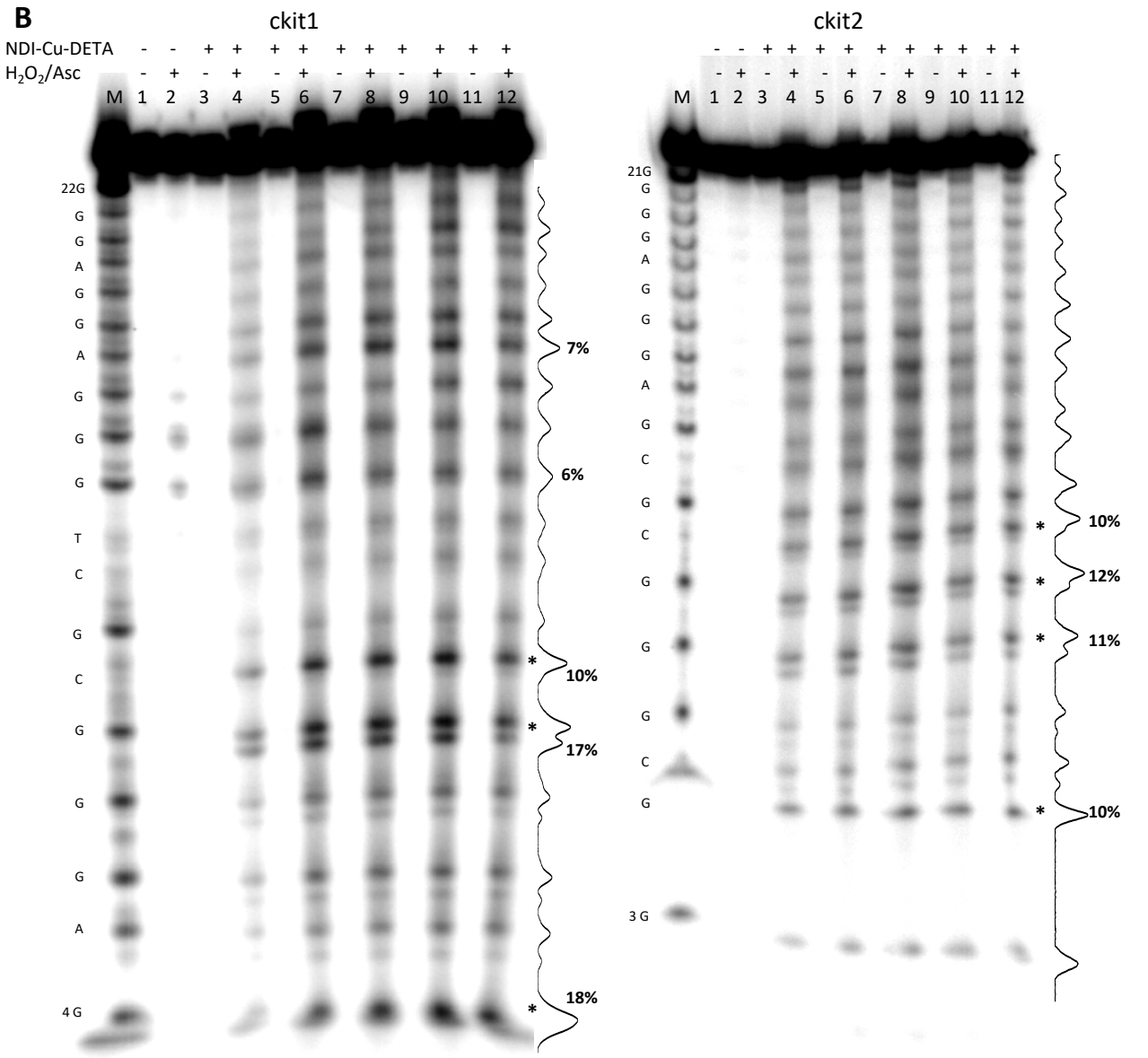

Figure S11. G4 cleavage of **NDI-Cu-DETA** on A) c-myc and bcl-2 B) c-kit1 and c-kit2. Denaturing polyacrylamide gels of cleavage products in presence of the compound. Oligonucleotides (0.25 µM) were reacted with increasing amount (0.78 – 25 µM in A), lanes 3-14) (1.56 – 25 µM in B), lanes 3-12) of NDI-Cu-DETA for 2.5 min in presence of 1 mM sodium ascorbate (Asc) and 1 mM hydrogen peroxide (H_2O_2). Control samples in the presence only of ascorbate and in the absence of **NDI-Cu-DETA** and hydrogen peroxide were included (lanes 2). Samples were run on denaturing polyacrylamide gels. Asterisks highlight major cleavage sites, M=marker lane. Panels include intensity profiles of lanes 14 in A) and 12 in B) and quantification of the major bands (%).

Table S5. Summary of **NDI-Cu-DETA** cleavage sites on all tested G4 oligonucleotides. Bold bases indicate sites of site-specific cleavage (higher than 20% of total cleavage sites); underlined bases indicate sites of multi-site/unspecific cleavage (lower than 20%). H stand for hybrid, A for antiparallel and P for parallel. Cleavage folds were calculated as the total cleavage bands in **NDI-Cu-DETA-**treated sample on the corresponding untreated sample (Fig. 2 and S11) and the resulting value was reported to that of ds scrambled hTel22.

G4	**Topology**	**Cleavage folds**	
LTR-III	H	8.2	GGG**A**GGCGTGGC**CT**GGGCGGGACTGGGG
un2	A	9.5	GGGGGCGAGGGG**C**GGGAGGGGGCGAGGGG
gp054b	H	7.4	GGGGTTGGGG**T**TGGGGTTGGGG
gp054e	H	7.7	GGGGCTGGGG**C**TGGGGTTGGGG
LTR-IV	P	6.0	TGGGCGGGACTGGGGAGTGGT
hTel22	H	2.5	AGGGTTAGGGTTAGGGTTAGGG
c-myc	P	4.0	TGAGGGTGGTGAGGGTGGGGAAGG
bcl-2	P	4.0	GGGCGCGGGAGGAAGGGGGCGGG
c-kit1	P	7.3	AGGGAGGGCGCTGGGAGGAGGG
c-kit2	P	12.8	CGGGCGGGCGCGAGGGAGGGG
ss scr hTel22	unstructured	1.7	

Ligand degradation under oxidative conditions

NDI-Cu-DETA complex is very stable in physiological buffer conditions (pH 7.4) at 37°C and remains unchanged over a week (t_R = 5.8 min).

In DNA cleavage studies, however, oxidative conditions have been used, but no significant ligand modifications can be defined at gel reaction time (around 2.5-3 min), confirming that G4s are targeted by unmodified NDI-Cu-DETA (Figure S10).

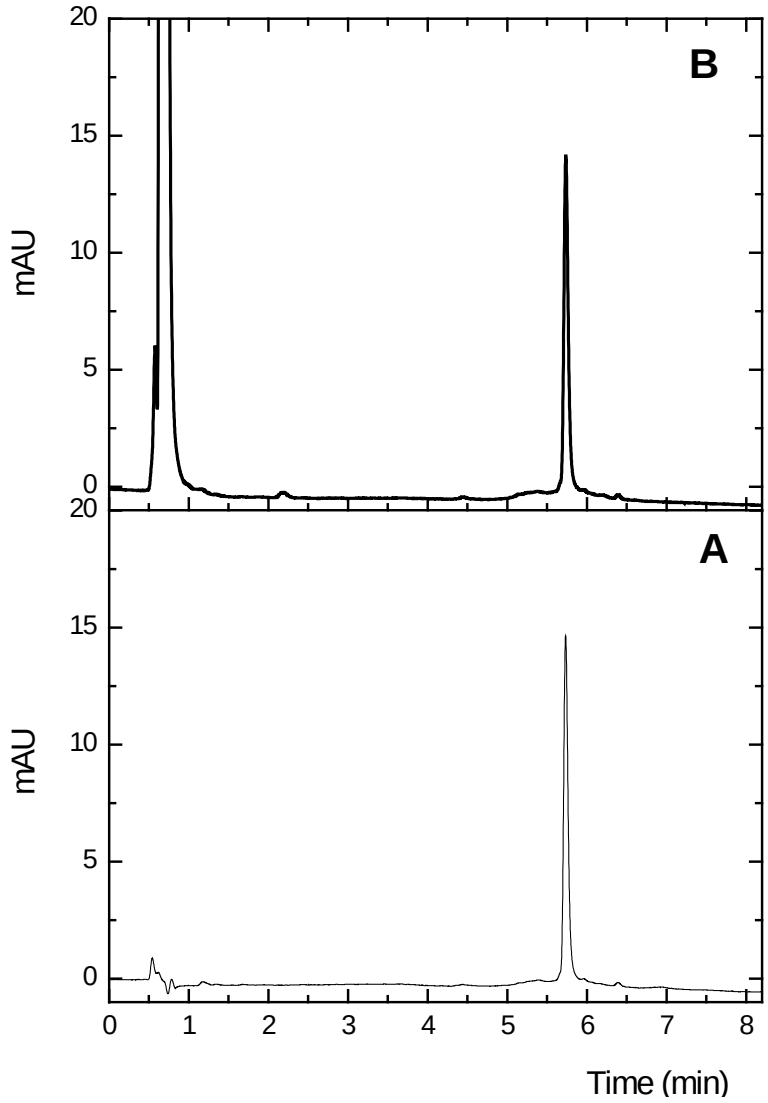

Figure S12. HPLC elution profiles of (A) NDI-Cu-DETA (6.25 µM)-LTR-III (12.5 µM) complex in 10 mM phosphate buffer at pH 7.4 and (B) after the addition of ascorbate (1 mM) and H_2O_2 (1mM).

If we follow the oxidative reactions for long time (around 2 h), it is possible identify two principal degradation compounds of our ligand at 6.27 min (DEG-1) and 6.40 min (DEG-2) respectively (Figure S11 and Scheme 2).

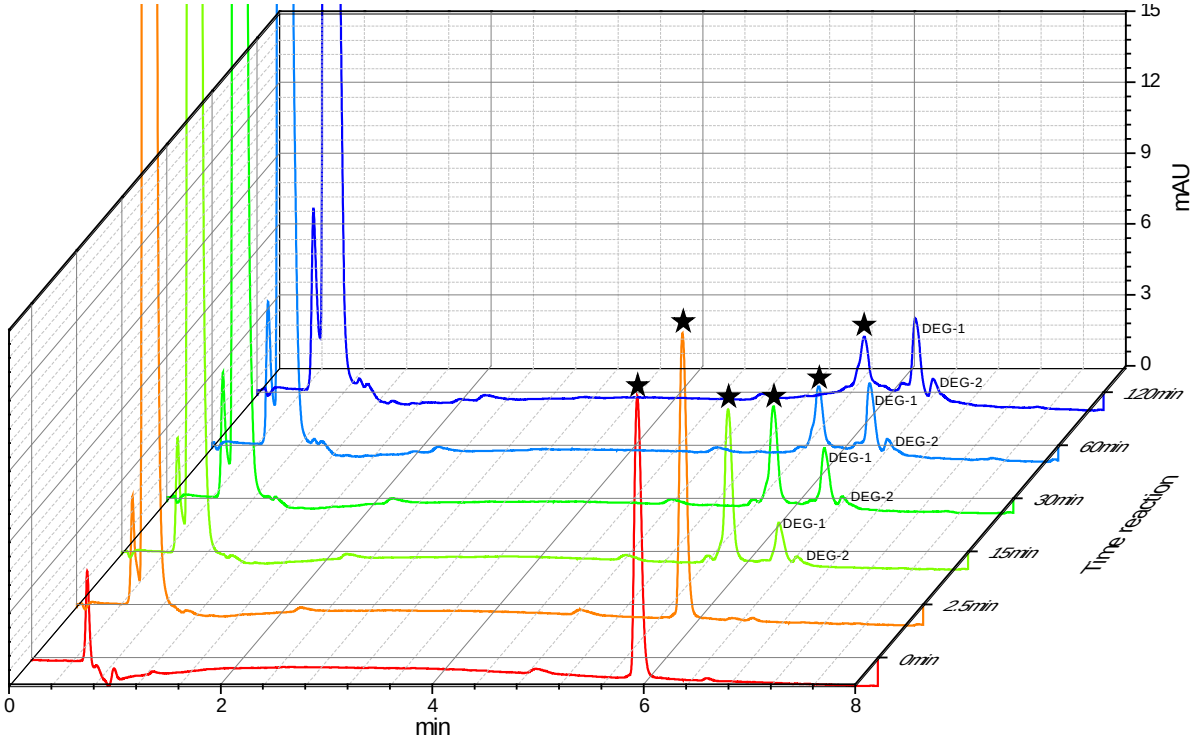

Figure S13. HPLC elution profiles of NDI-Cu-DETA (6.25 µM)-LTR-III (12.5 µM) complex (0 min) and after the addition of ascorbate (1 mM) and H_2O_2 (1mM) in 10 mM phosphate buffer at pH 7.4 followed over time for 2 h. Star indicates the NDI-Cu-DETA –LTR-III complex.

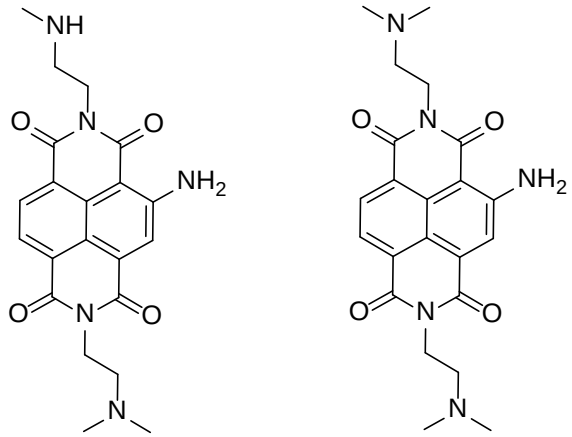

DEG-1 **DEG-2**

Scheme S2 - Degradation products of NDI-Cu-DETA under oxidative conditions

These products are also identified by adding H_2O_2 and ascorbic acid in the buffer solution that contains only NDI-Cu-DETA complex without G4s. It is important to note that the presence of folded G4s favours the formation and stabilization of compound **DEG-1** rather than compound **DEG-2**, while the lack of G4s induces the formation of **DEG-2** as the main product.

Analysis of NDI-Cu-DETA reactivity towards G bases by hot piperidine.

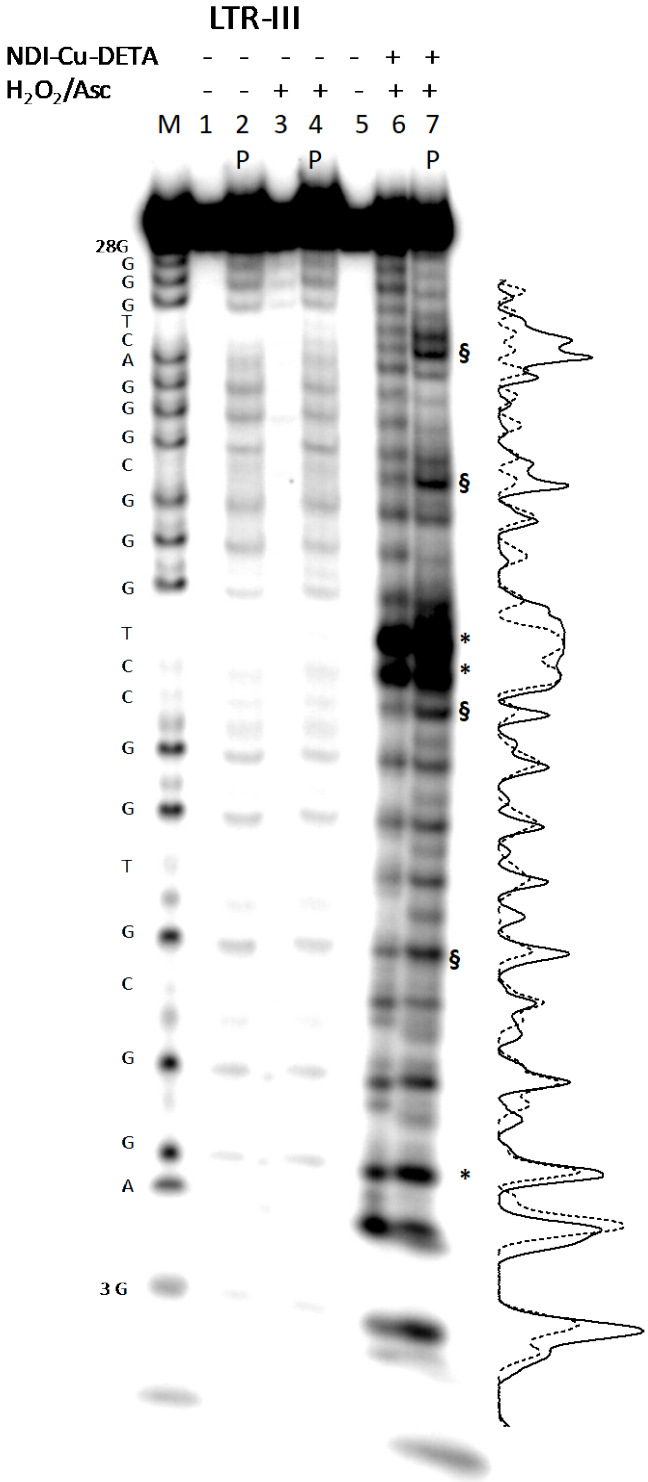

Figure S14. Analysis of **NDI-Cu-DETA** reactivity towards G bases by hot piperidine. Oligonucleotide LTR-III (0.25 µM) was reacted with 12.5 µM of **NDI-Cu-DETA** for 2.5 min in the presence of 1 mM sodium ascorbate (Asc) and 1 mM hydrogen peroxide (H_2O_2). Samples were then treated with 1 M hot piperidine (P) for 30 min at 90 °C (lanes 2, 4 and 7). Samples were run on denaturing polyacrylamide gels. Asterisks highlight major cleavage sites, § symbols indicate cleavage sites enhanced by piperidine treatment, M=marker lane. Intensity profiles are referred to lane 6 (dashed line) and lane 7 (solid line).

Role of hydrogen peroxide on the reactivity of NDI-Cu-DETA

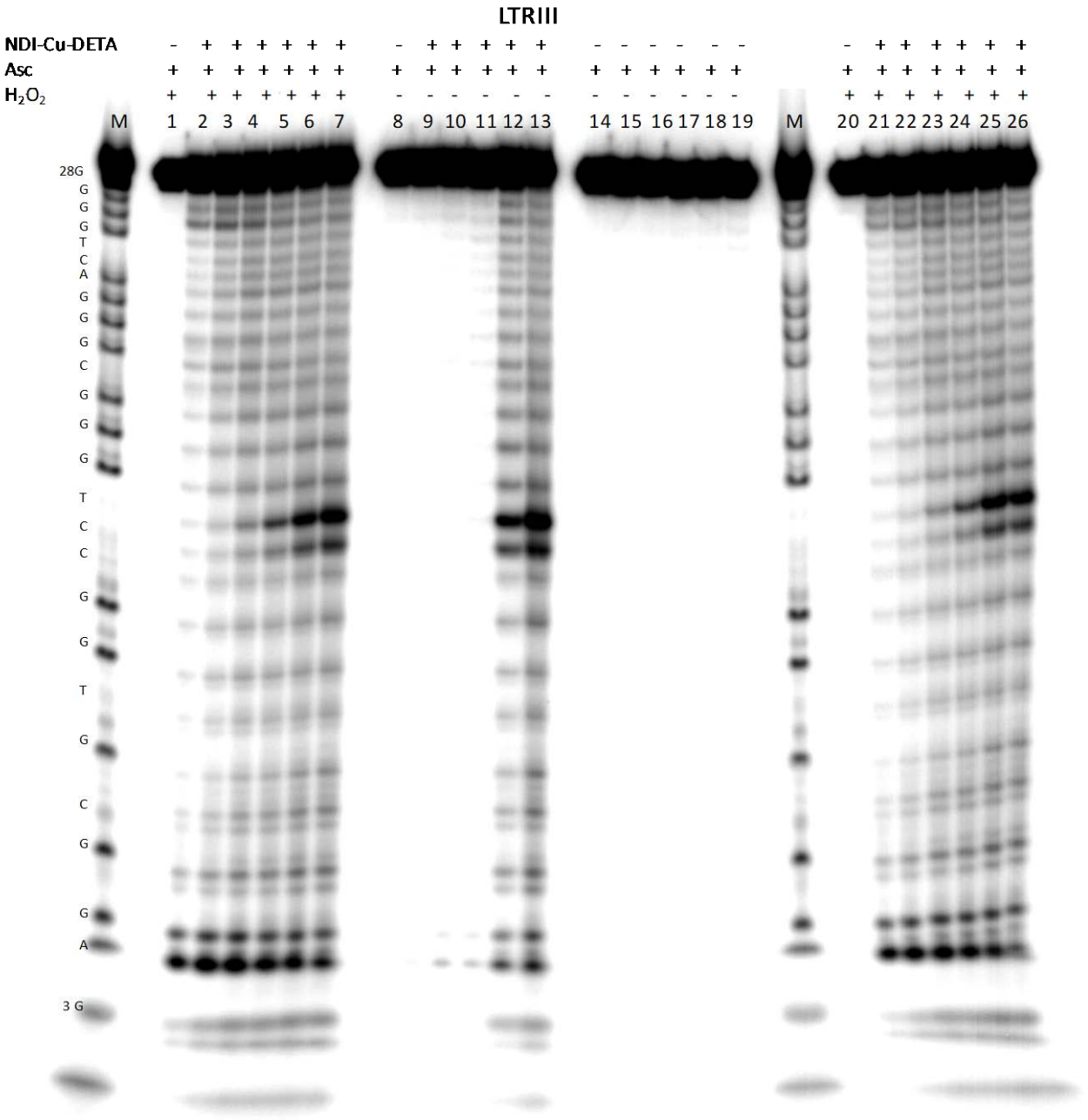

Figure S15. NDI-Cu-DETA-induced cleavage on G4 oligonucleotides in the absence of H_2O_2 or presence of the ROS scavenger mannitol. Oligonucleotide LTR-III (0.25 µM) was reacted with increasing amounts (0.78 - 12.5 µM) of **NDI-Cu-DETA** for 2.5 min in the presence of 1 mM sodium ascorbate (Asc) and 1 mM hydrogen peroxide (H_2O_2) (lanes 1-7), or in the absence of H_2O_2 for 30 min (lanes 8-13), or in the presence of 100 x mannitol, a radical scavenger (lanes 20-26). Control samples in the presence only of ascorbate and in the absence of **NDI-Cu-DETA** and hydrogen peroxide were included (lanes 14-19). Samples were run on denaturing polyacrylamide gels. Asterisks highlight major cleavage sites, M=marker lane.

MS characterization of NDI-Cu-DETA cleavage products

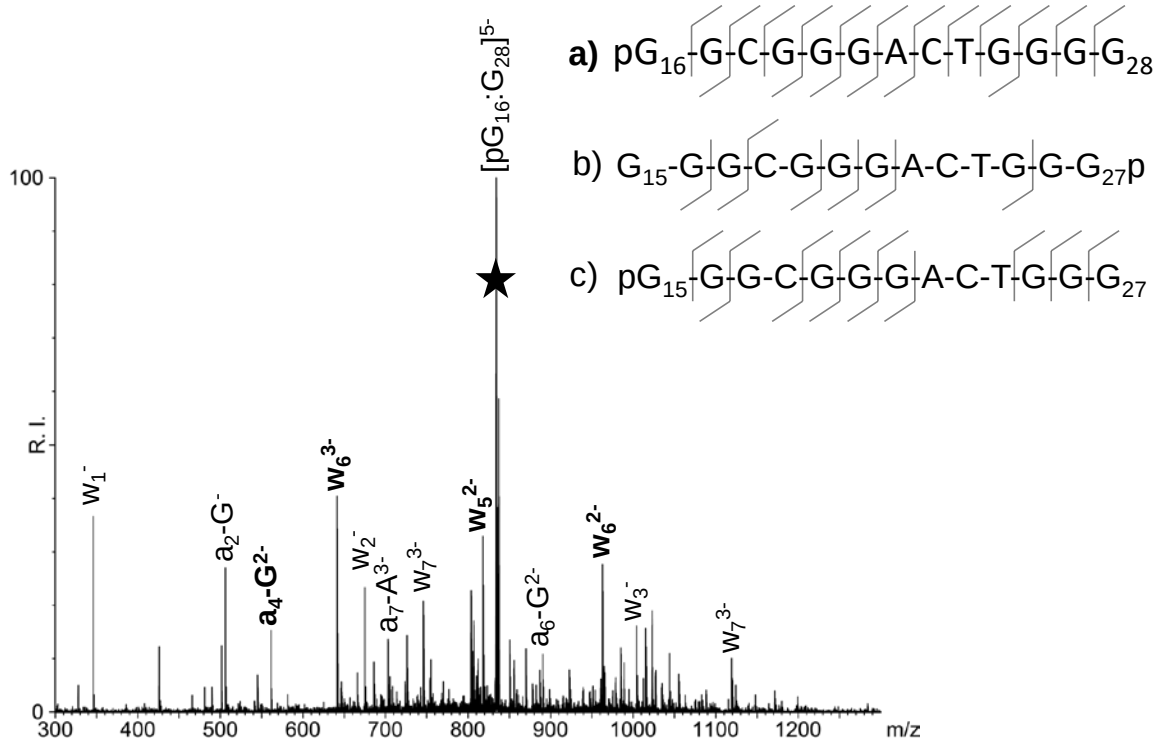

Figure S16. MS characterization of **NDI-Cu-DETA** cleavage products. Oligonucleotide LTR-III (0.25 µM) was reacted with 12.5 µM of **NDI-Cu-DETA** for 2.5 min in the presence of 1 mM sodium ascorbate and 1 mM hydrogen peroxide. One of the most intense band (C13+T14) (see Fig. 3A) was excised and the cleavage products were extracted and analyzed by MS and MS/MS. In the representative example the mass of the parent ion ($[pG_{16}{:}G_{28}]^{5-}$, m/z 833.929^{5-}, neutral monoisotopic mass 4174.7 Da) is consistent with the three sequences (a, b, c). The most intense fragment ions belong to the sequence **a)** that have the higher coverage, also intense fragments (bold label) are diagnostic to sequence **a)** that is then assigned to the peak 833.929^{5-}.

MS detection of NDI-Cu-DETA-induced oxidation of G4s

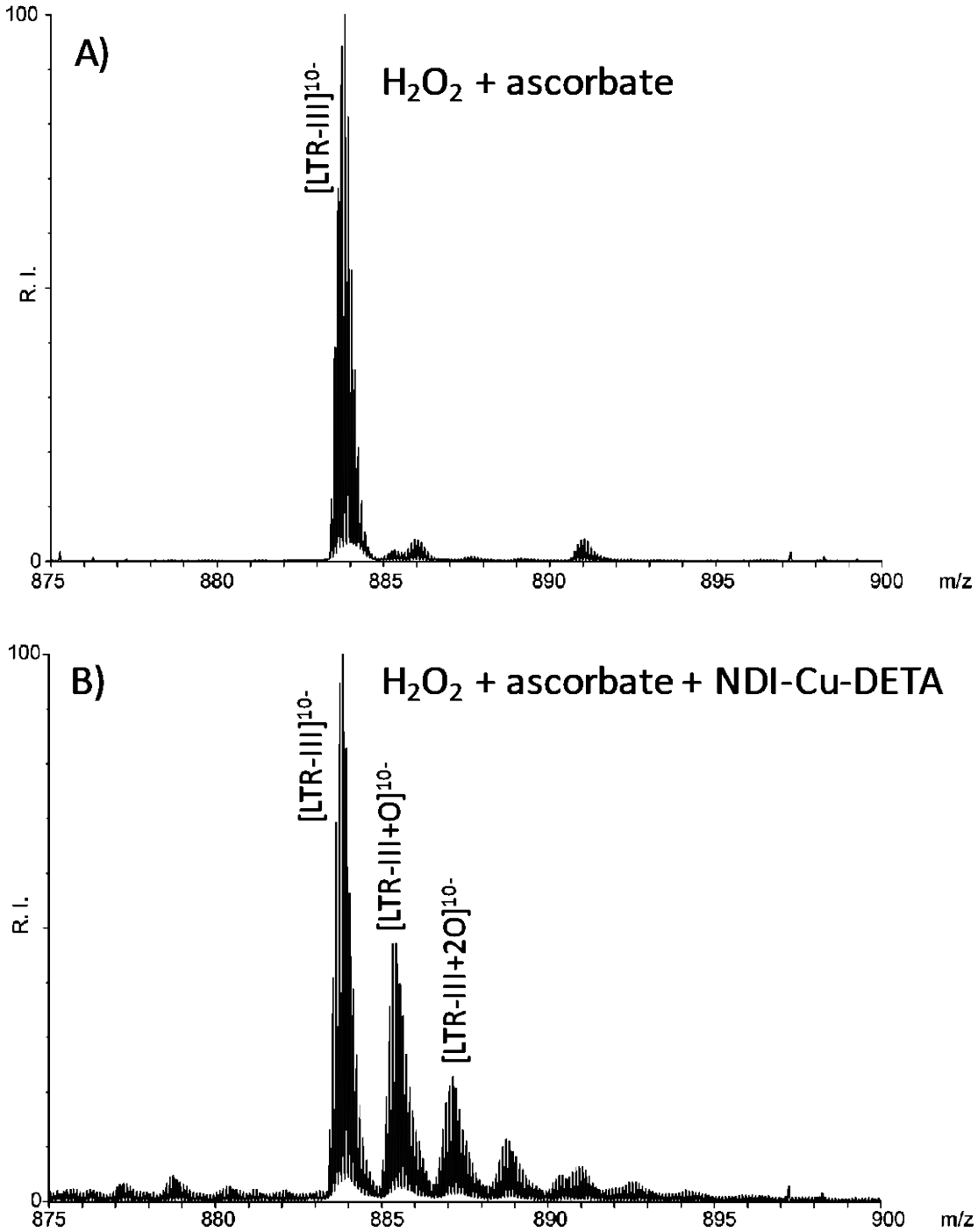

Figure S17. MS detection of **NDI-Cu-DETA**-induced oxidation of G4s. Oligonucleotide LTR-III (0.25 µM) was incubated with 1 mM sodium ascorbate and 1 mM hydrogen peroxide A) or with 1 mM sodium ascorbate, 1 mM hydrogen peroxide in the presence of 12.5 µM of **NDI-Cu-DETA** B) for 2.5 min. The bands corresponding to the uncleaved LTR-III were excised, extracted and analyzed by MS. The spectra are zoomed to show the $[LTR\text{-}III]^{10-}$ ion and the oxygen adducts. Only the treatment with NDI-Cu-DETA oxidizes the LTR-III G4s.

MS detection of NDI-Cu-DETA-induced oxidation of guanosine monophosphates.

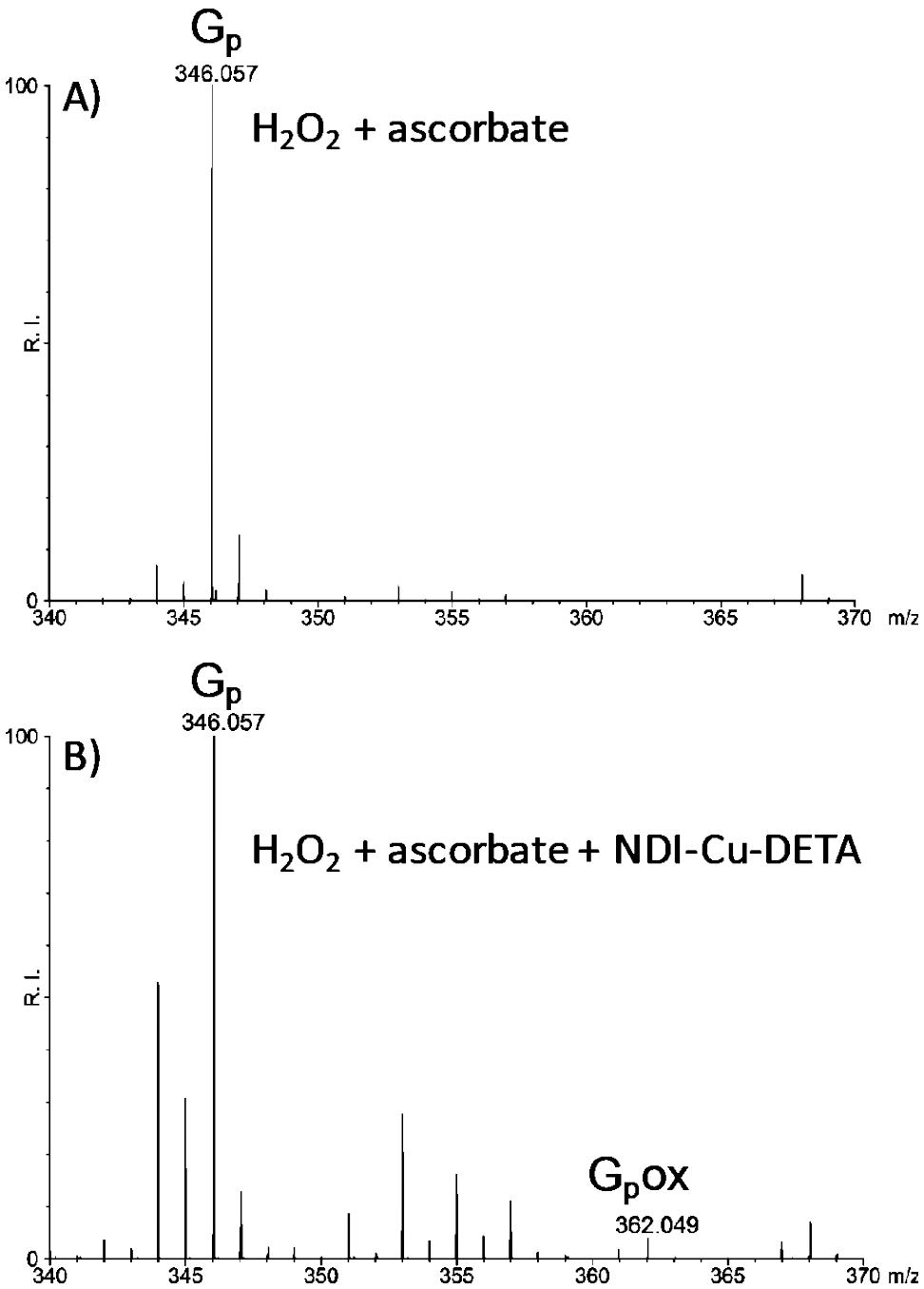

Figure S18. MS detection of **NDI-Cu-DETA**-induced oxidation of guanosine monophosphates. Oligonucleotide LTR-III (0.25 µM) was incubated with 1 mM sodium ascorbate and 1 mM hydrogen peroxide A) or with 1 mM sodium ascorbate, 1 mM hydrogen peroxide in the presence of 12.5 µM of **NDI-Cu-DETA** B) for 2.5 min. The bands corresponding to the uncleaved LTR-III were excised, extracted, digested with S1nuclease and analyzed by MS. Only the treatment with NDI-Cu-DETA induces guanosine oxidation.

Representative MS spectrum of NDI-Cu-DETA:G4 complexes

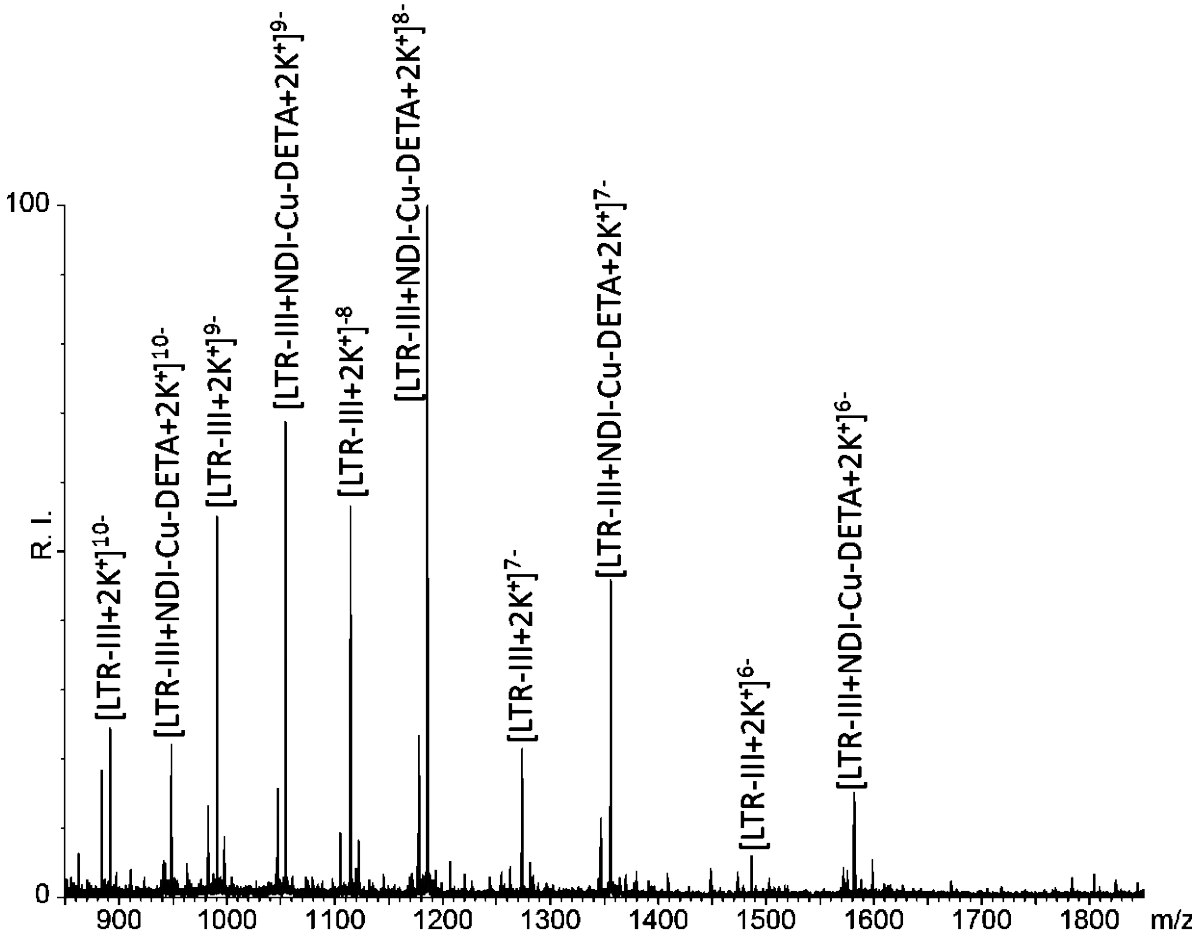

Figure S19. Representative MS spectrum of **NDI-Cu-DETA**:G4 complexes. Oligonucleotide LTR-III (5 µM) incubated with NDI-Cu-DETA at molar ratio 1:2 in HFIP/TEA pH 7.4 added of 0.8 mM KCl and 20% IPA was analyzed by ESI-MS. The reconstructed-ion chromatogram area for each species was used to calculate the MS-derived binding affinities listed in Table S6.

Table S6. MS-derived fraction-bound % of **NDI-Cu-DETA** and G4 oligonucleotides.

Oligo	Stoichiometry **NDI-Cu-DETA**:oligo	Fraction-bound %
LTR-III	1:1	58.6
un2	1:1	32.8
LTR-IV	1:1	21.6
hTel22	1:1	19.8
gp054b	1:1	10.7
gp054e	1:1	7

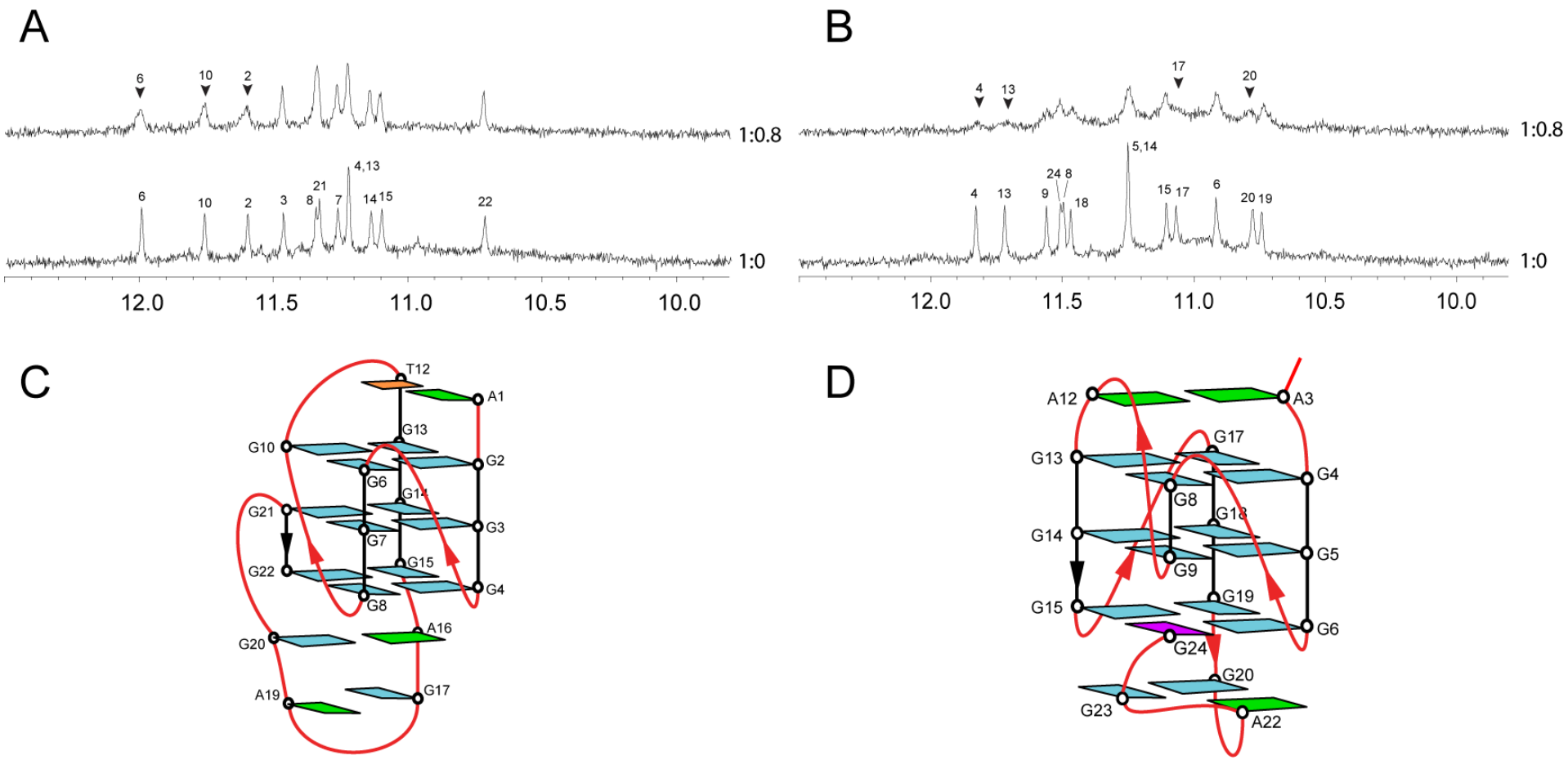

Figure S20. Imino proton spectra of A) c-kit1 and B) c-myc G-quadruplex DNA free and bound with NDI-Cu-DETA at 1:0.8 ratio in presence of 0.2 fraction of EDTA. The black arrows indicate the guanine imino proton peaks that were significantly broadened during the titration of NDI-Cu-DETA towards the G-quadruplexes. Schematic of C) c-kit1 (Phan A.T., Kuryavyi V., Burge S., Neidle S., Patel D.J. (2007). J. Am. Chem. Soc., 129, 4386-4392.) and D) c-myc (Phan A.T., Kuryavyi V., Gaw H.Y., Patel D.J. (2005). Nat. Chem. Biol., 1, 167-173.) DNA G-quadruplexes. The binding of the compound to c-kit1 results in broadening of G6, G10 and G2, indicating the top tetrad as the first binding site. The significant cleavage at G13 and C9 might be related to this binding site, while the major cleavage occurred around G4, G8 and A16 (Fig. S11B) might be related to an additional binding site near the bottom tetrad or/and coexistence of an additional conformation. The binding of the compound to c-myc results in broadening of G4, G13 and G17, as well as G20, indicating top tetrad and bottom triad binding sites respectively. These binding sites are consistent with the cleavage data showing major cleavage occurred in a top tetrad residue G4 (10%) and around bottom triad residues A21-G24 (31%) (Fig. S11A).

Molecular modeling

Cu-DETA geometry optimization Cartesian coordinates:

Atom type	X / Å	Y / Å	Z / Å
C	0.77100000	3.45300000	0.02100000
C	1.80200000	2.40500000	0.03500000
C	1.43500000	1.03700000	0.01400000
C	0.06500000	0.62900000	-0.01900000
C	-0.93700000	1.65800000	-0.07900000
C	3.14500000	2.78800000	0.07000000
C	2.48400000	0.07800000	0.02000000
C	3.82900000	0.48000000	0.04800000
C	4.92000000	-0.53200000	0.04300000
C	3.21300000	-2.34300000	-0.03800000
C	2.14000000	-1.30600000	-0.01700000
C	0.83800000	-1.70900000	-0.03600000
C	-0.27200000	-0.77500000	-0.00300000
H	0.64700000	-2.77300000	-0.07400000
H	3.37000000	3.84900000	0.08900000
O	2.97200000	-3.54100000	-0.07900000
O	6.10000000	-0.21500000	0.07300000
O	-2.18800000	1.46900000	-0.18000000
O	1.02300000	4.65100000	0.05000000
N	-0.56100000	2.99300000	-0.03900000
N	4.53200000	-1.88500000	-0.00200000
N	-1.52400000	-1.22500000	0.05600000
C	-1.83800000	-2.66100000	0.00800000
H	-1.63900000	-3.05900000	-0.99700000
H	-1.24100000	-3.23500000	0.72700000
C	4.16200000	1.83500000	0.07600000
H	5.20700000	2.11900000	0.09900000
C	-3.32400000	-2.79400000	0.32800000
H	-3.69200000	-3.79300000	0.04600000
H	-3.48400000	-2.69400000	1.41800000
N	-4.02600000	-1.79200000	-0.46700000
C	-5.49600000	-1.72000000	-0.22300000
H	-5.98900000	-1.61500000	-1.20000000
H	-5.86200000	-2.65300000	0.23200000
Cu	-3.13900000	-0.19600000	-0.10900000
C	-5.73900000	-0.49400000	0.63300000
H	-6.78300000	-0.14100000	0.61400000
H	-5.49400000	-0.71000000	1.68000000
N	-4.82500000	0.58000000	0.17100000
H	-5.12500000	0.84200000	-0.77700000
C	-1.63226490	4.00024907	-0.08001014
H	-1.19018327	5.00230461	-0.12080883
H	-2.25239036	3.91086221	0.81925089
H	-2.25239036	3.83805244	-0.96902795
C	5.58009189	-2.91705989	-0.01602800
H	6.56544102	-2.43720518	-0.00950570
H	5.47786876	-3.52930434	-0.91931265
H	5.47786876	-3.55362893	0.87028249

HPLC PURITY DATA:

Analytical Method

flow rate of 1 mL/min; loop 10 μL; λ_{obs} = 256 nm

t (min)	H_2O 0.1% TFA	MeCN
0	95.0	5.0
2	95.0	5.0
11	63	37
15	63	37

Preparative Method

flow rate of 30 mL/min; loop 10 mL

t (min)	H_2O 0.1% TFA	MeCN
0	95.0	5.0
2	95.0	5.0
14	80	20
20	80	20

NDI- DETA (2):

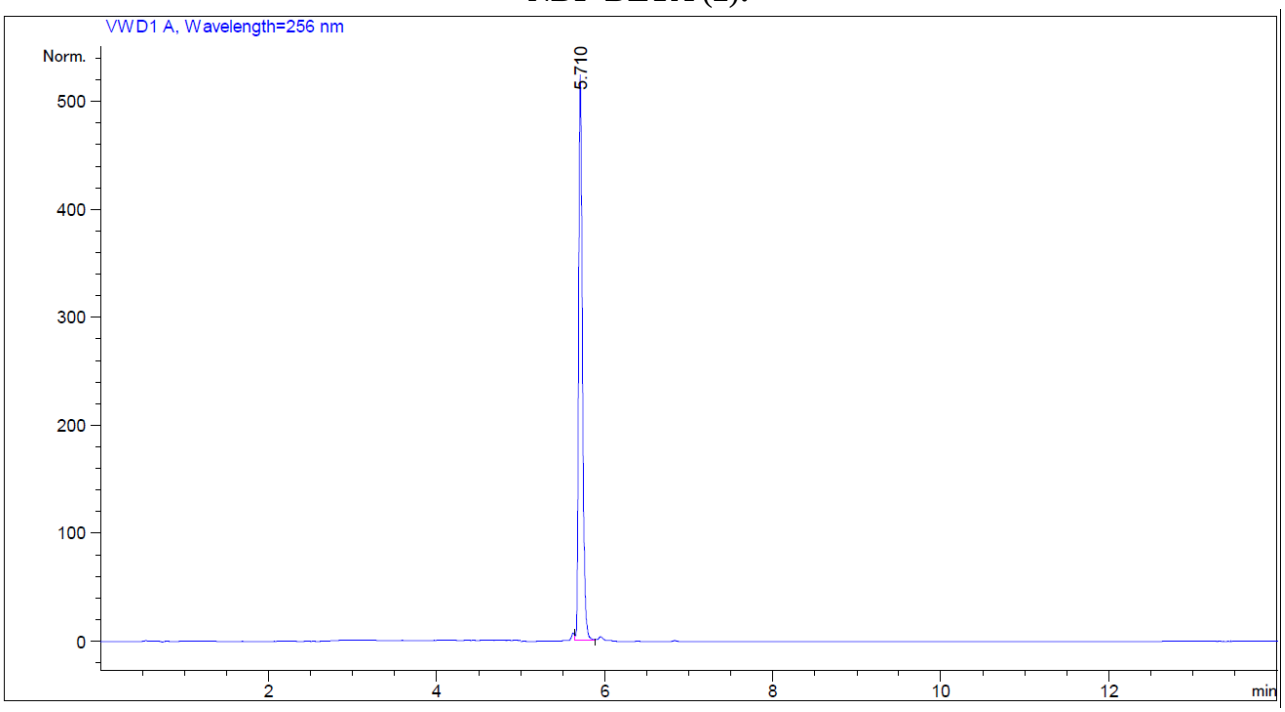

DEG-1*:*

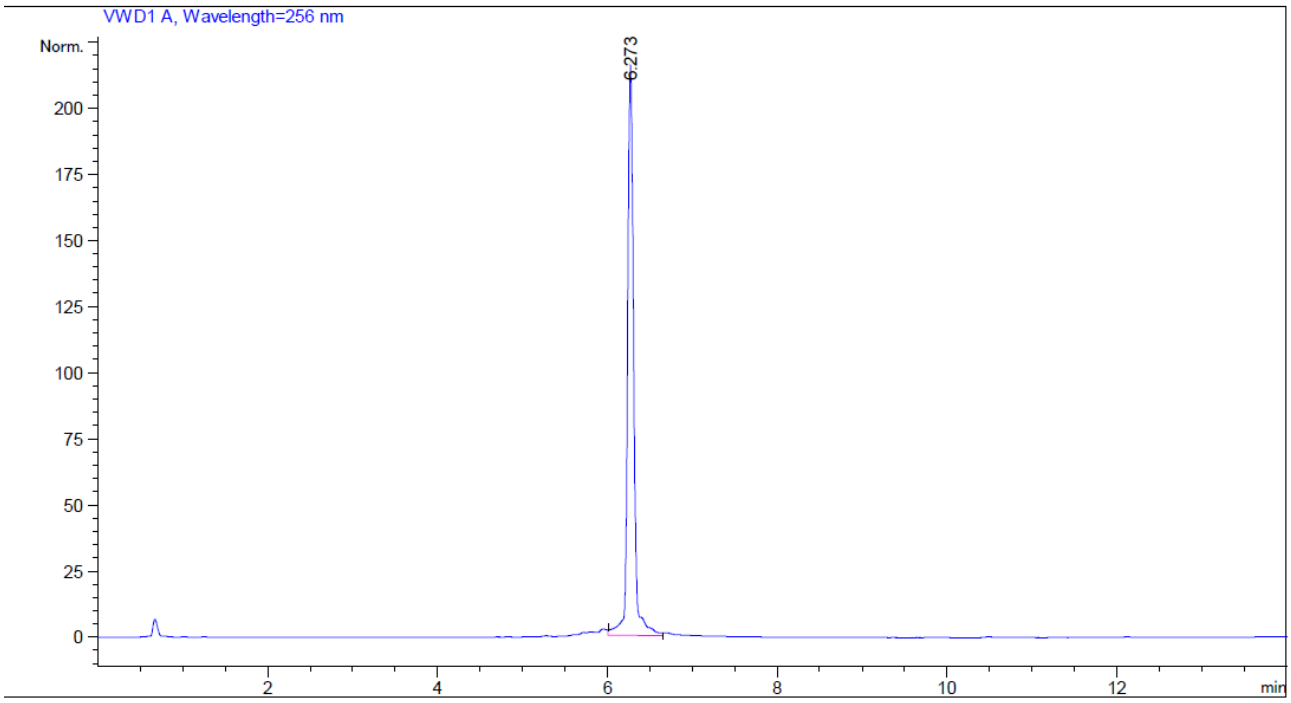
VWD1 A, Wavelength=256 nm
Norm.
6.273
200
175
150
125
100
75
50
25
0
2
4
6
8
10
12
min

DEG-2*:*

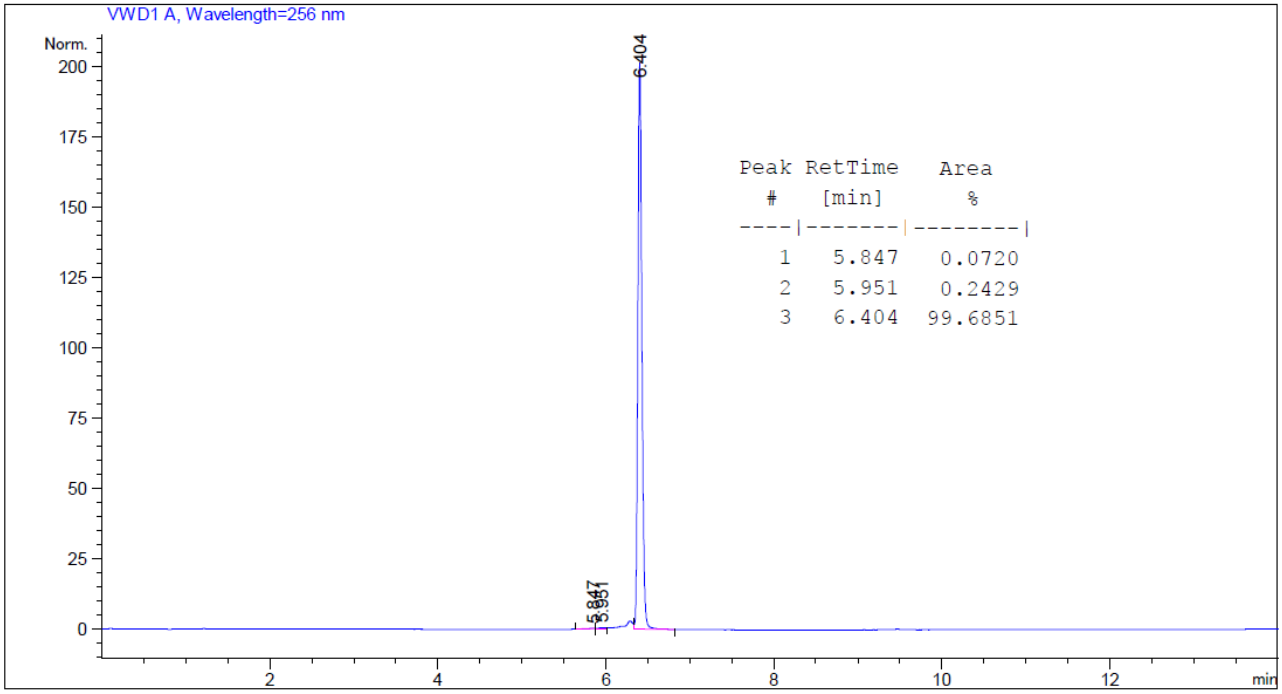
VWD1 A, Wavelength=256 nm
Norm.
6.404
5.847
5.951
200
175
150
125
100
75
50
25
0
2
4
6
8
10
12
min
Peak RetTime Area
[min] %
1 5.847 0.0720
2 5.951 0.2429
3 6.404 99.6851

Mass Spectra:

NDI-DETA (2)

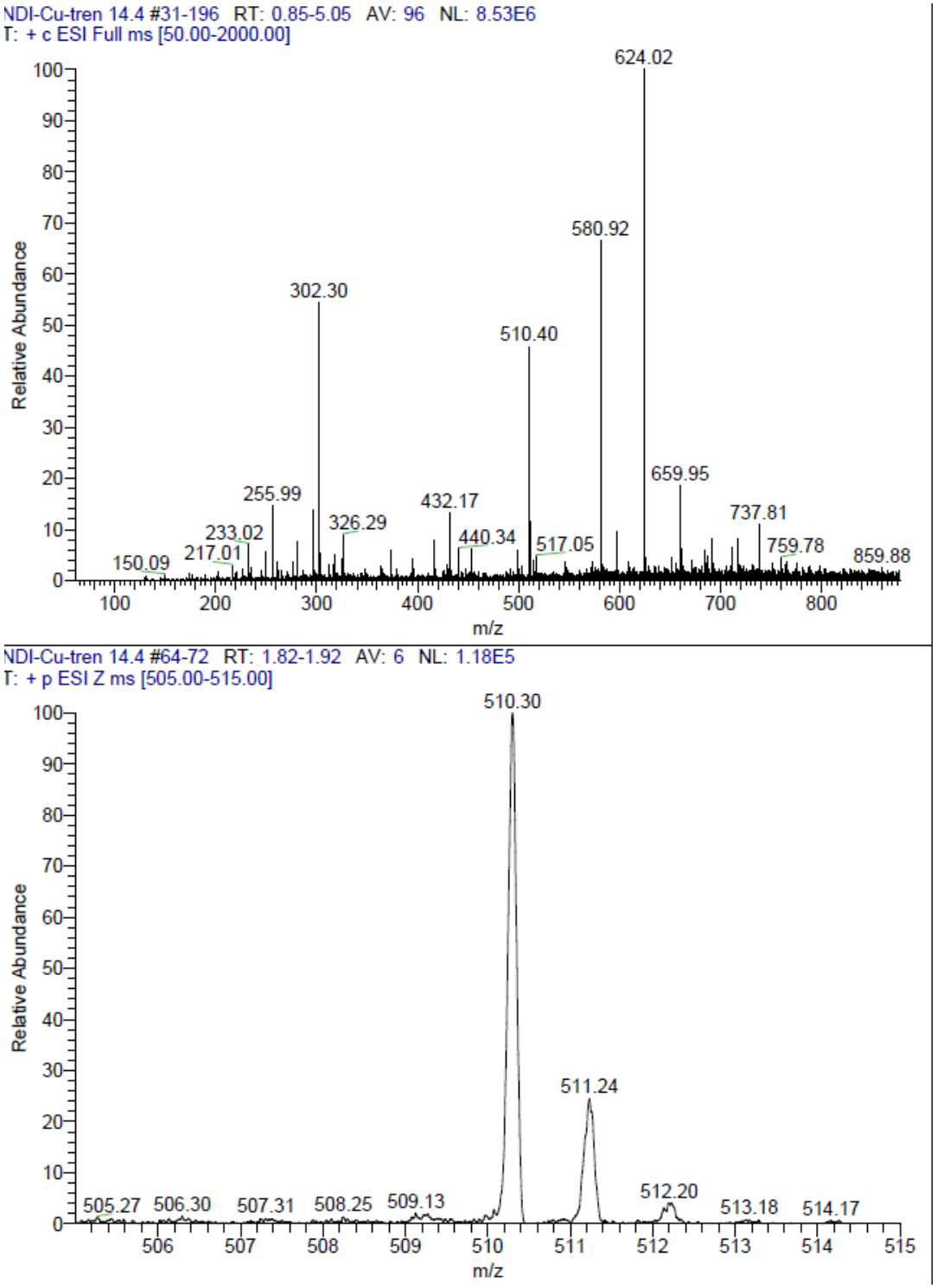

NDI- Cu-DETA (3)

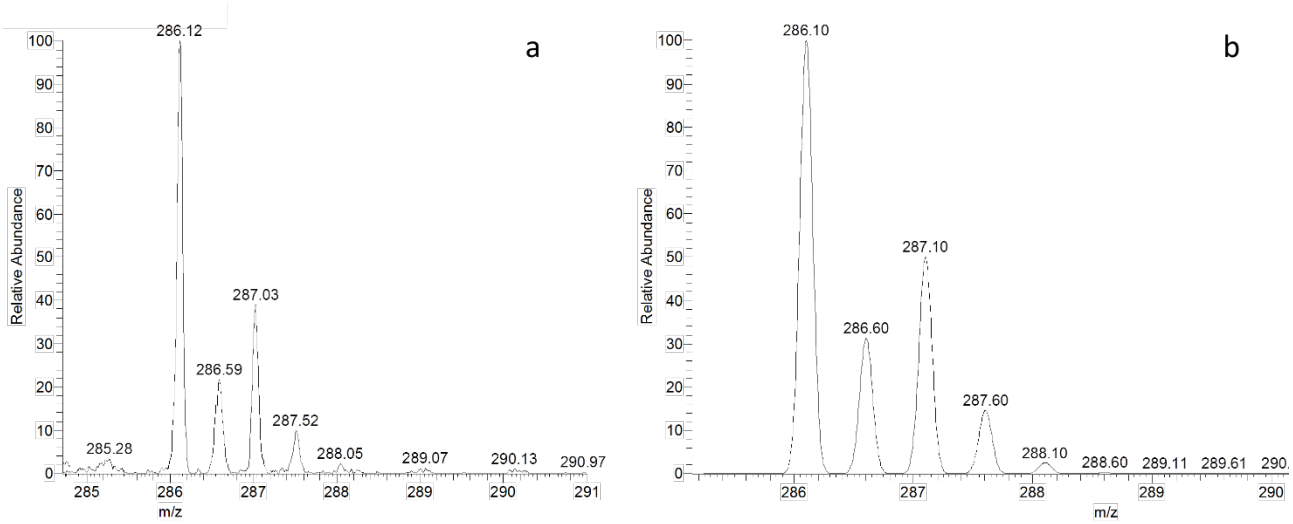

Figure S21. (a) Experimental and (b) simulated ESI(+)-MS peak at 286.10 m/z, corresponding to the di-charged complex $[NDIH\text{-}Cu\text{-}DETA]^{2+}$.

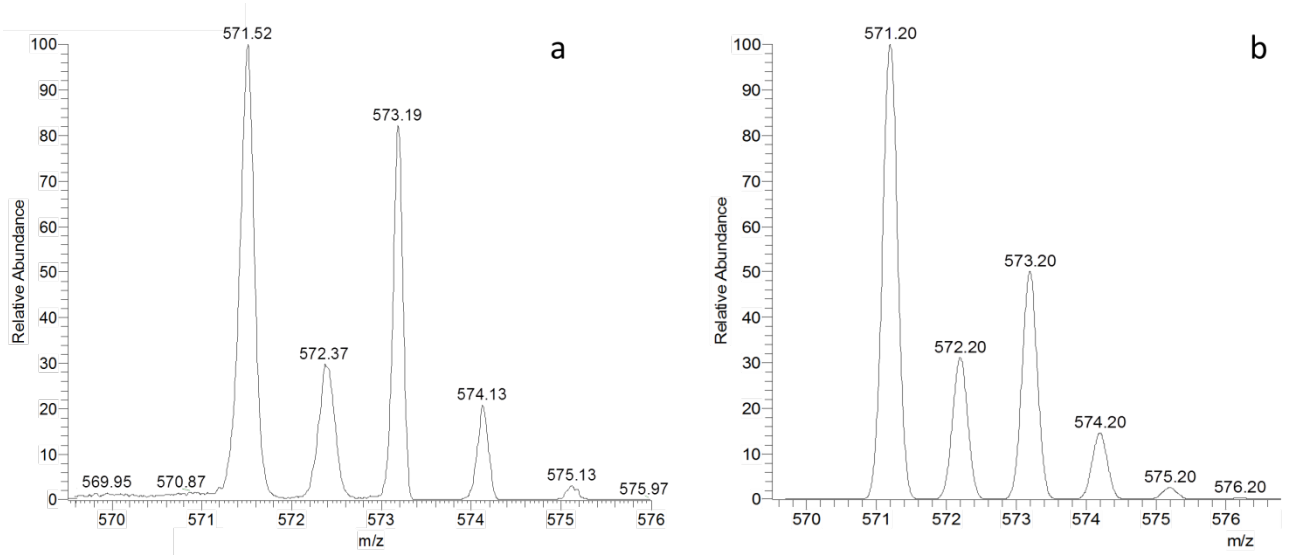

Figure S22. (a) Experimental and (b) simulated ESI(+)-MS peak at 571.52 m/z, corresponding to the mono-charged complex $[NDI\text{-}Cu\text{-}DETA]^{+}$.

DEG-1

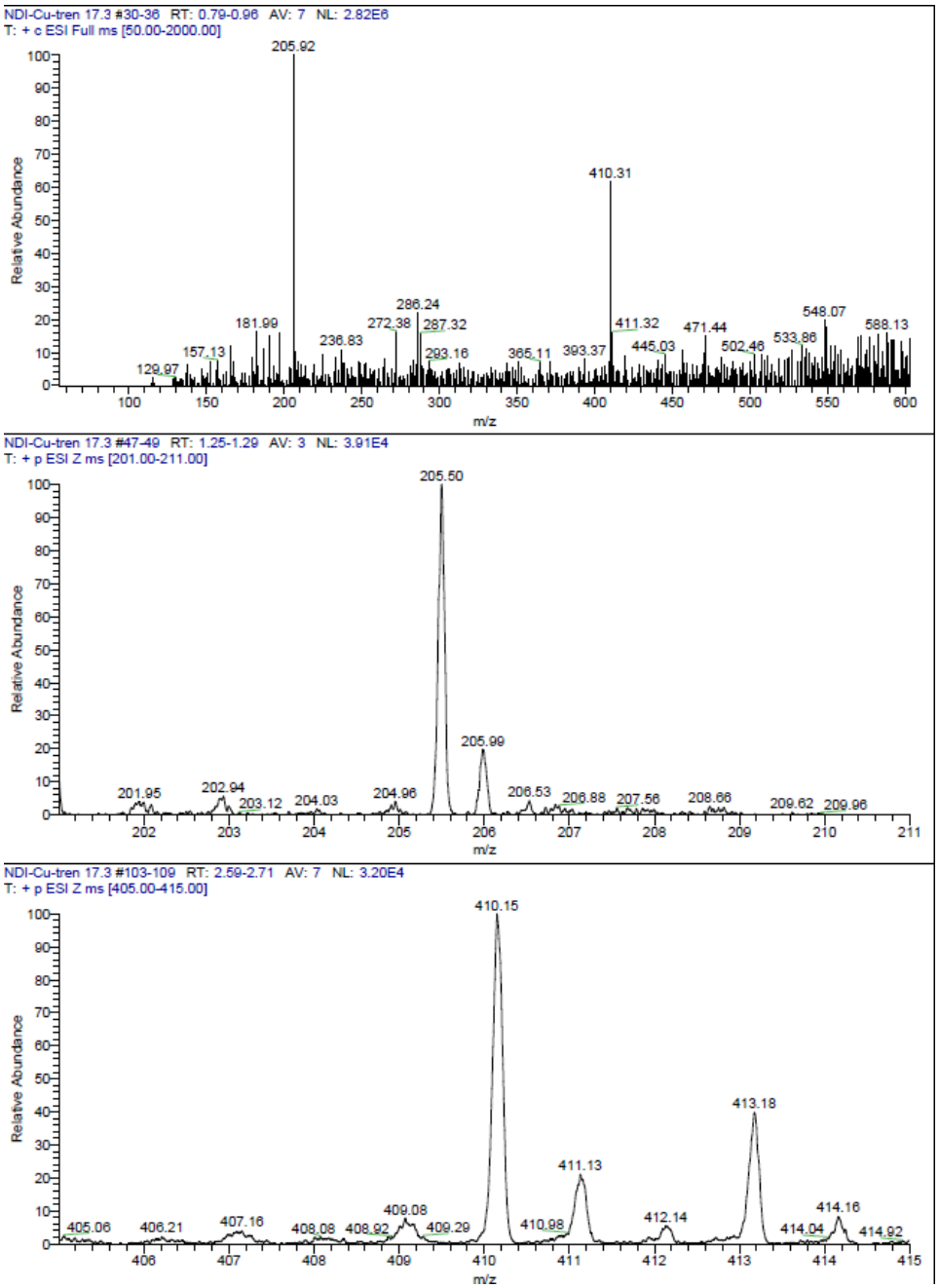
NDI-Cu-tren 17.3 #30-36 RT: 0.79-0.96 AV: 7 NL: 2.82E6
T: + c ESI Full ms [50.00-2000.00]
205.92
410.31
286.24
272.38
287.32
181.99
236.83
157.13
129.97
293.16
365.11
393.37
411.32
445.03
471.44
502.46
533.86
548.07
588.13
Relative Abundance
m/z
NDI-Cu-tren 17.3 #47-49 RT: 1.25-1.29 AV: 3 NL: 3.91E4
T: + p ESI Z ms [201.00-211.00]
205.50
205.99
201.95
202.94
203.12
204.03
204.96
206.53
206.88
207.56
208.66
209.62
209.96
Relative Abundance
m/z
NDI-Cu-tren 17.3 #103-109 RT: 2.59-2.71 AV: 7 NL: 3.20E4
T: + p ESI Z ms [405.00-415.00]
410.15
413.18
411.13
409.08
414.16
405.06
406.21
407.16
408.08
408.92
409.29
410.98
412.14
414.04
414.92
Relative Abundance
m/z

DEG-2

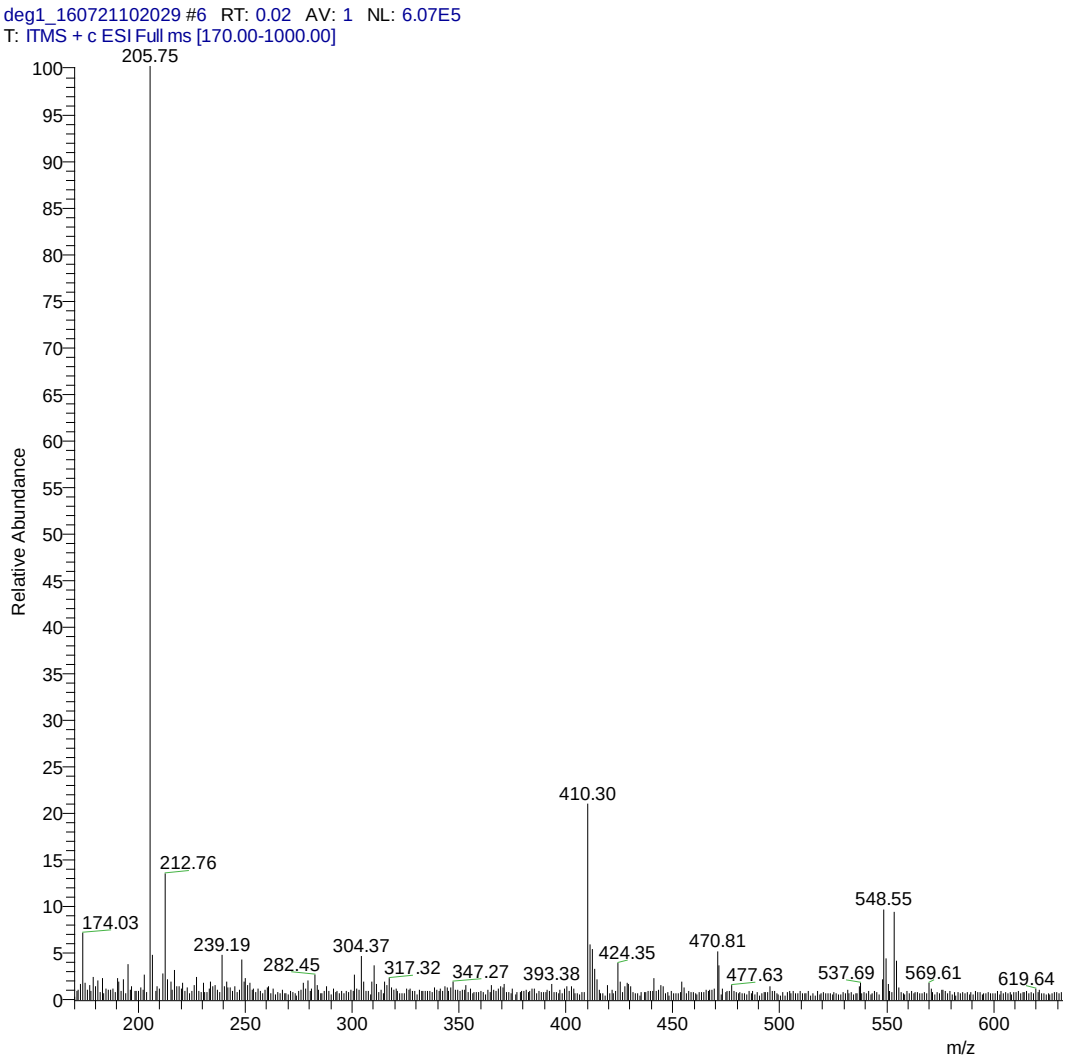
deg1_160721102029 #6 RT: 0.02 AV: 1 NL: 6.07E5
T: ITMS + c ESI Full ms [170.00-1000.00]
Relative Abundance
m/z
205.75
212.76
174.03
239.19
282.45
304.37
317.32
347.27
393.38
410.30
424.35
470.81
477.63
537.69
548.55
569.61
619.64

CD and FRET melting profiles

A

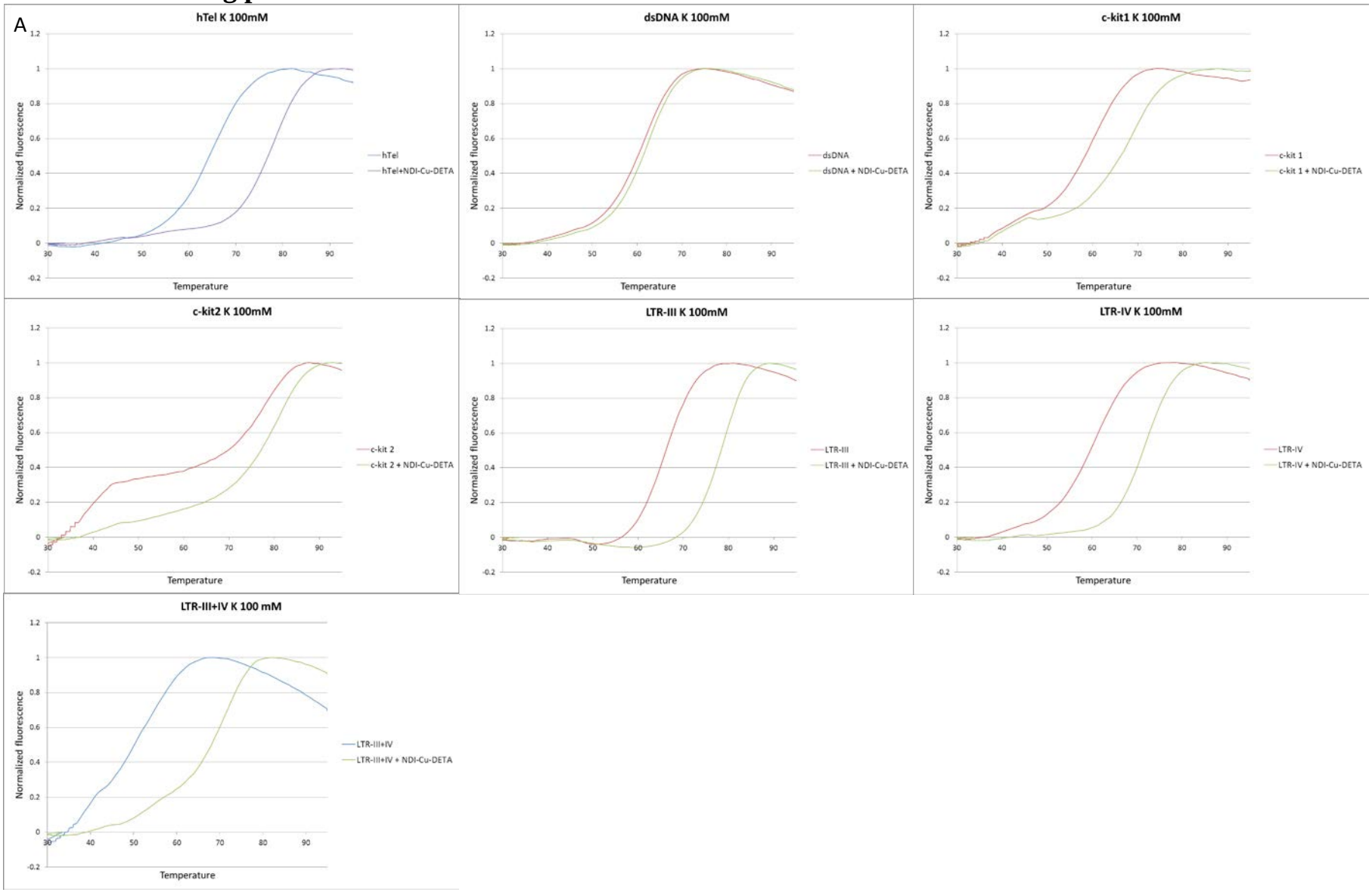

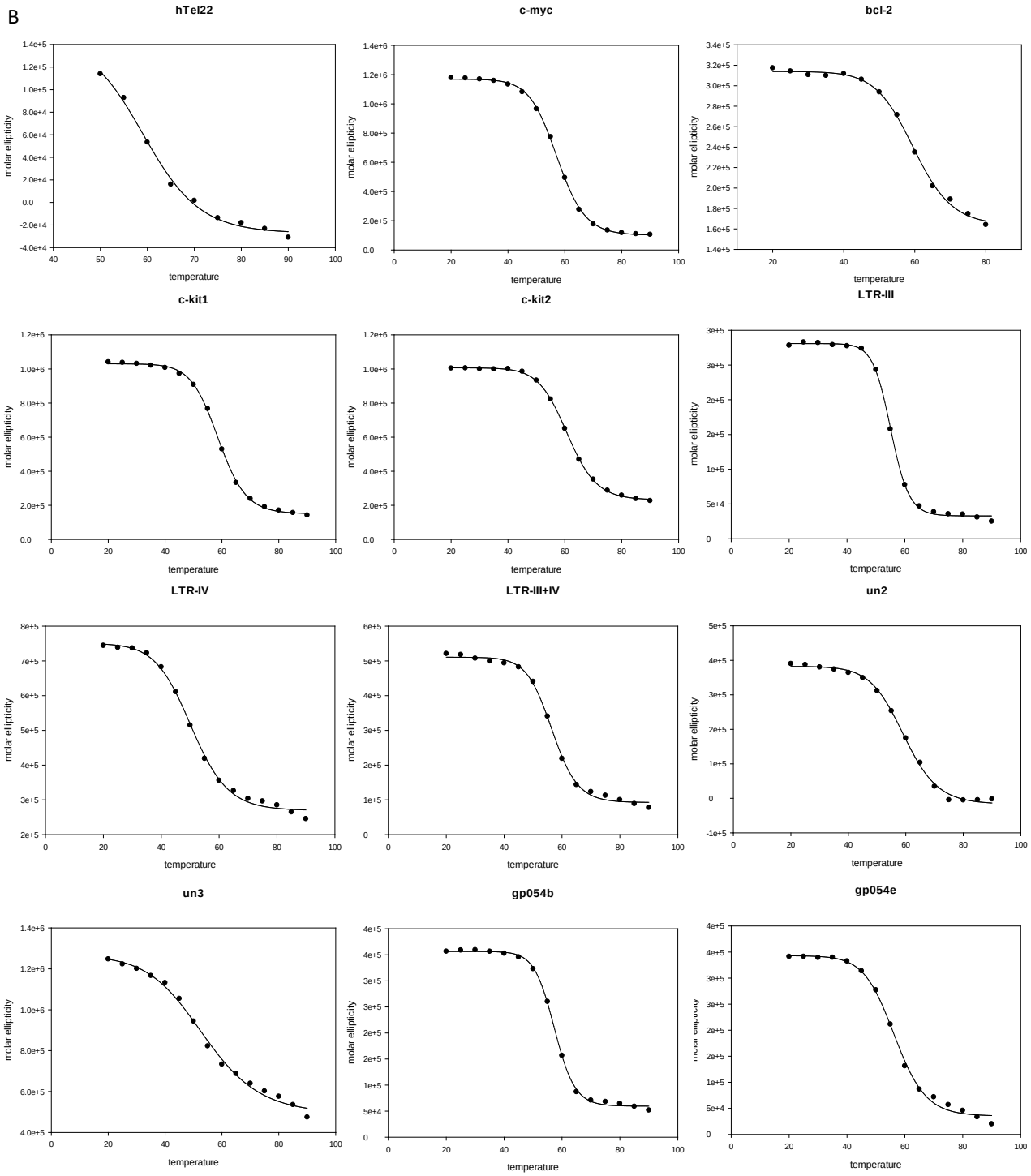

Figure S23. A) FRET and **B)** CD melting profiles of the oligonucleotides used in this work.

NMR Spectra:

***NDI- DETA* (2)**
($CDCl_3$) ^1H NMR 300MHz

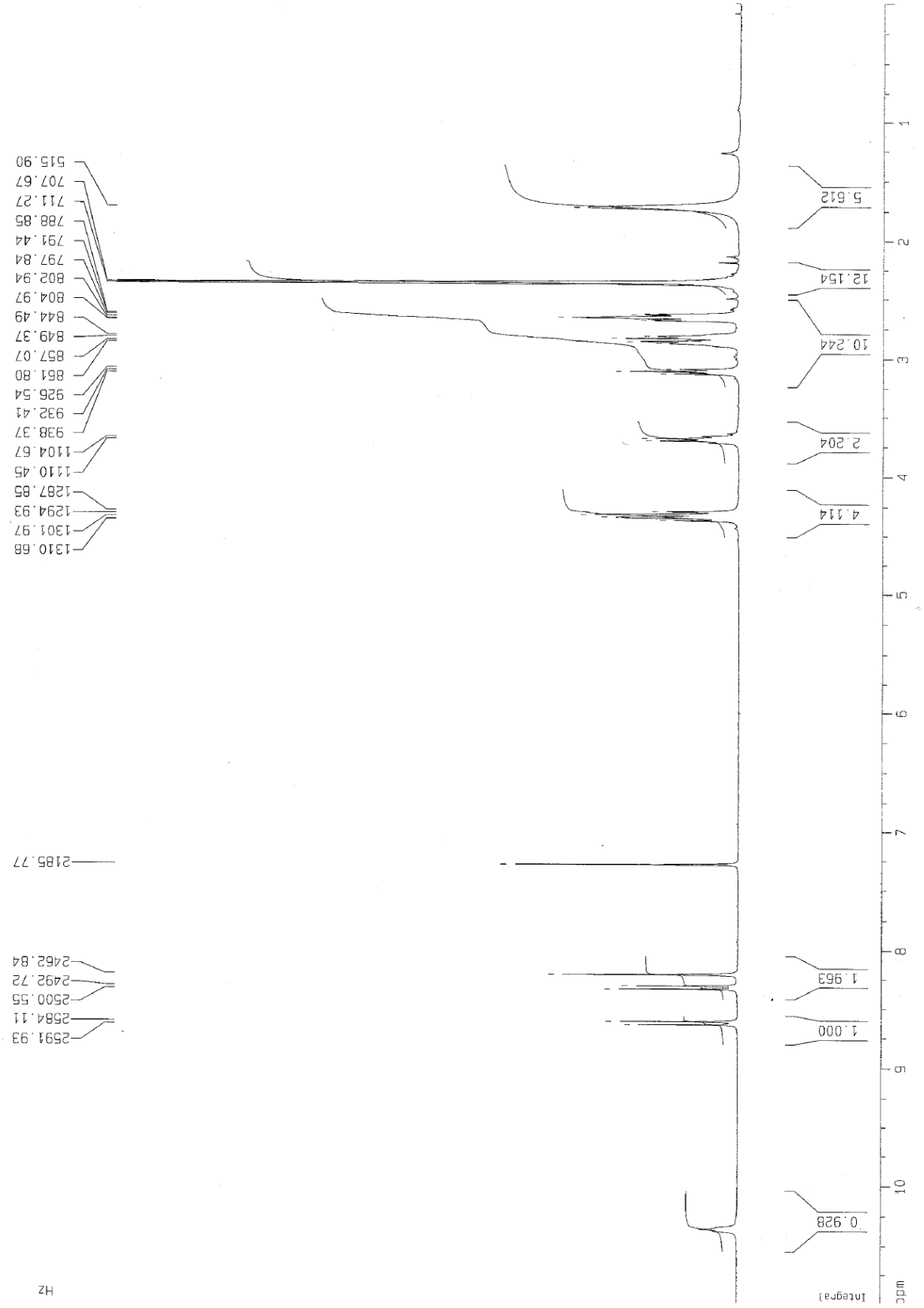

($CDCl_3$) ^{13}C NMR 75MHz

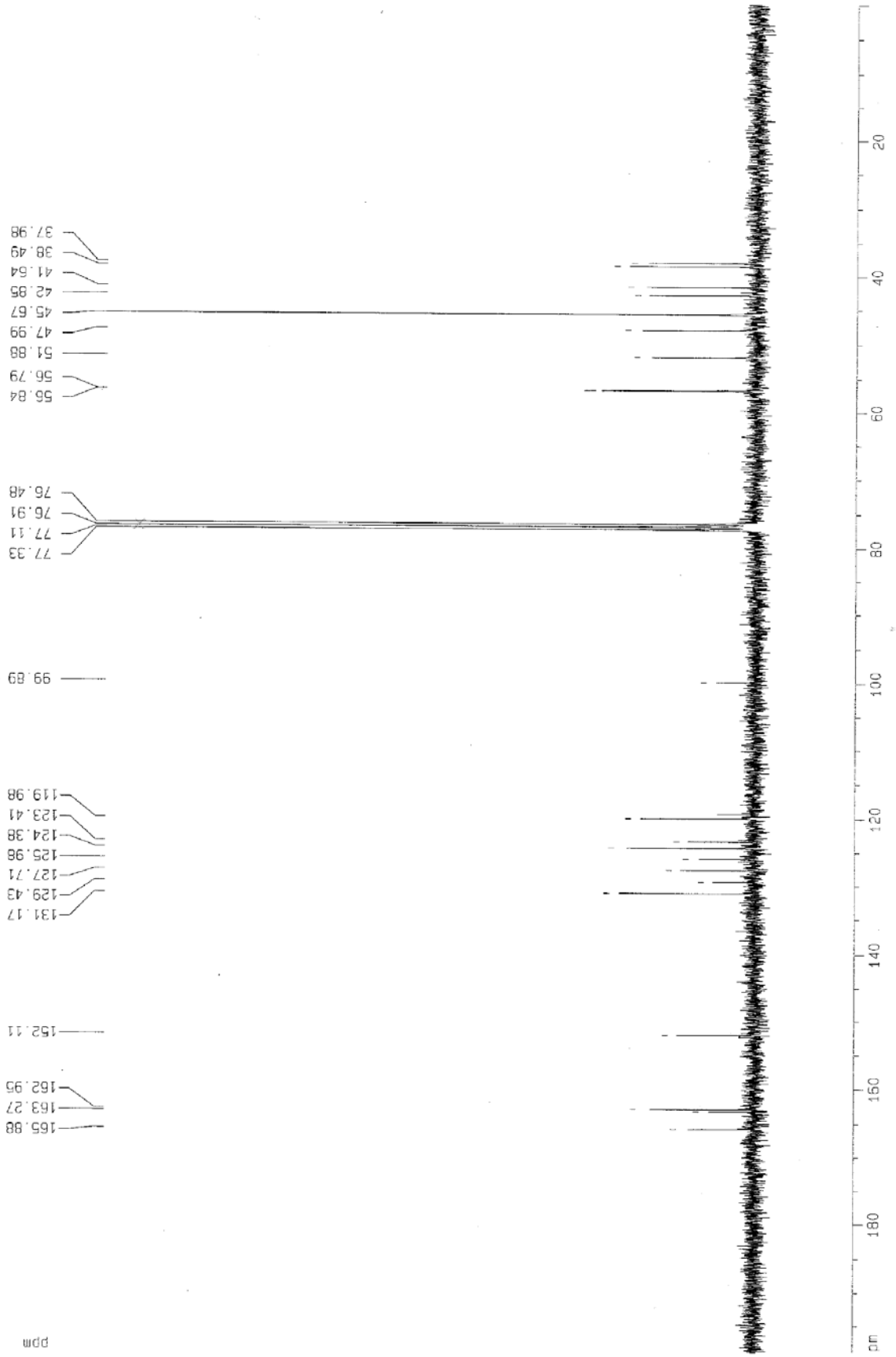

DEG-1

(CD_3OD) ^1H NMR 300MHz

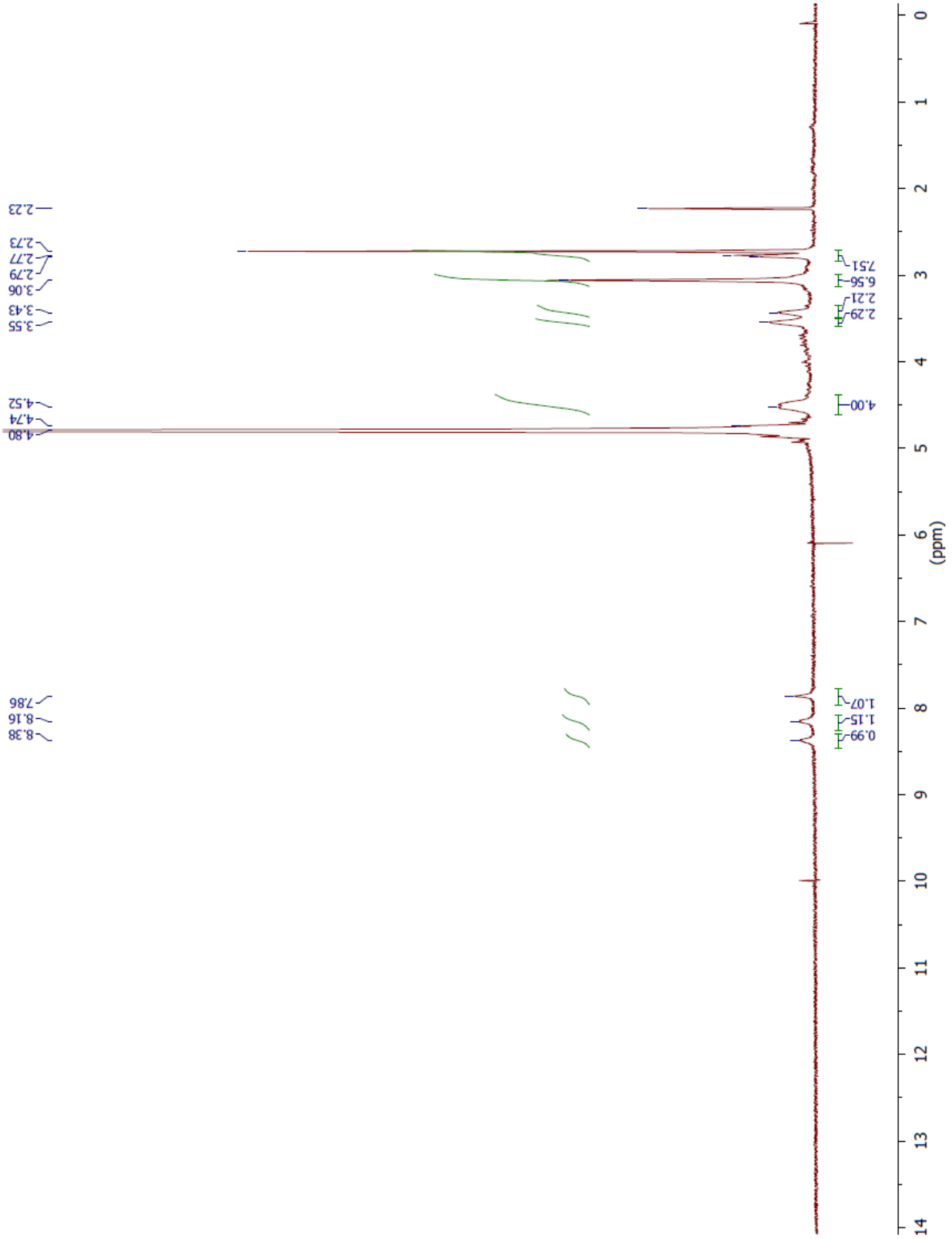

DEG-2

(CD_3OD) ^1H NMR 300MHz

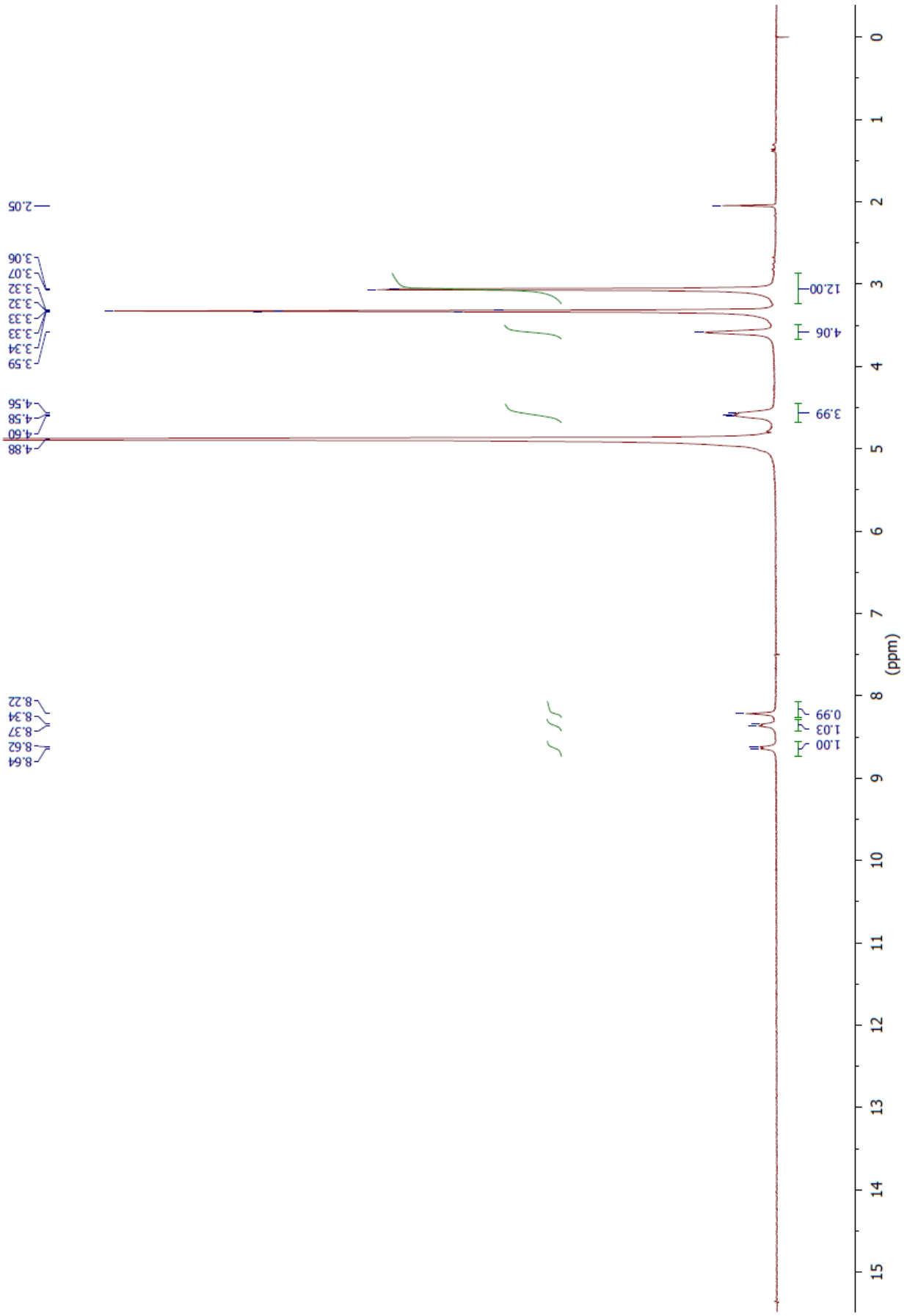

(CD_3OD) ^{13}C NMR 75MHz

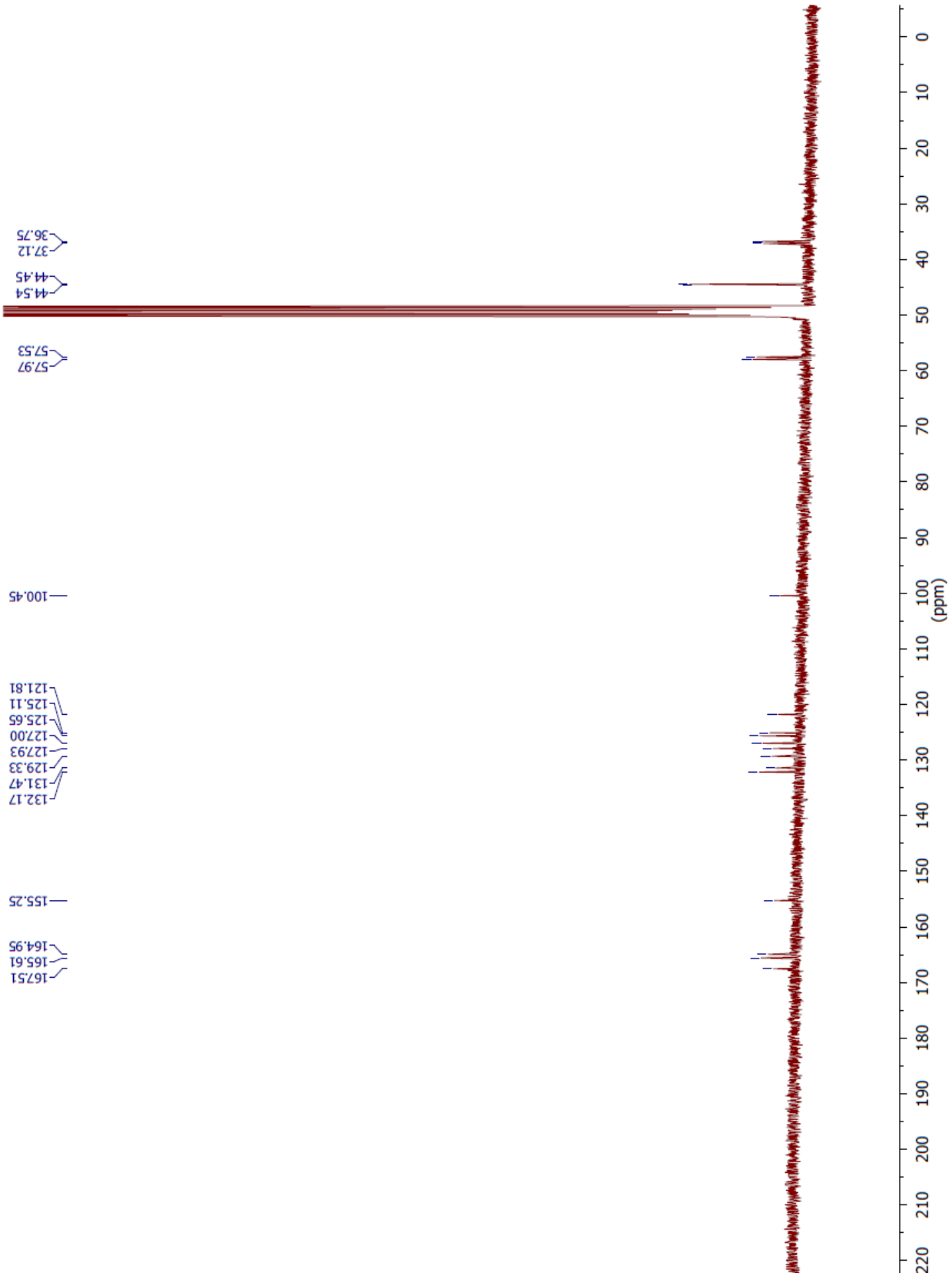

Supplementary References

S1. Doria, F.; Manet, I.; Grande, V.; Monti, S.; Freccero, M., Water-soluble naphthalene diimides as singlet oxygen sensitizers. *J. Org. Chem.* **2013**, *78*, 8065-73.

S2. Greenfield, N. J., Using circular dichroism collected as a function of temperature to determine the thermodynamics of protein unfolding and binding interactions. *Nat. Protoc.* **2006**, *1*, 2527-35.

S3. Rescigno, A.; Sanjust, E.; Soddu, G.; Rinaldi, A. C.; Sollai, F.; Curreli, N.; Rinaldi, A., Effect of 3-hydroxyanthranilic acid on mushroom tyrosinase activity. *Biochim. Biophys. Acta* **1998**, *1384*, 268-76.

S4. Minotti, G.; Aust, S. D., The requirement for iron (III) in the initiation of lipid peroxidation by iron (II) and hydrogen peroxide. *J Biol Chem* **1987**, *262*, 1098-104.

S5. Maxam, A. M.; Gilbert, W., Sequencing end-labeled DNA with base-specific chemical cleavages. *Methods Enzymol.* **1980**, *65*, 499-560.

S6. Perrone, R.; Doria, F.; Butovskaya, E.; Frasson, I.; Botti, S.; Scalabrin, M.; Lago, S.; Grande, V.; Nadai, M.; Freccero, M.; Richter, S. N., Synthesis, Binding and Antiviral Properties of Potent Core-Extended Naphthalene Diimides Targeting the HIV-1 Long Terminal Repeat Promoter G-Quadruplexes. *J. Med. Chem.* **2015**, *58*, 9639-52.

S7. Butovskaya, E.; Heddi, B.; Bakalar, B.; Richter, S. N.; Phan, A. T., The major G-quadruplex form of HIV-1 LTR reveals a (3+1) folding topology containing a stem-loop. J. *Am. Chem. Soc.* **2018**, *140*, 13654–13662.

S8. Gans, P.; Sabatini, A.; Vacca, A. Investigation of equilibria in solution. Determination of equilibrium constants with the HYPERQUAD suite of programs. *Talanta* **1996**, *43*, 1739-53.

S9. Doria, F.; Amendola, V.; Grande, V.; Bergamaschi, G.; Freccero, M., Naphthalene diimides as selective naked-eye chemosensor for copper(II) in aqueous solution. *Sensors and Actuators B: Chemical* **2015**, *212*, 137-144.

S10. Martell , A. E.; Smith , R. M., *Critical Stability Constants*. 1 ed.; Springer US: 1982; Vol. 5, p XVII, 604.

S11. Ambrus, A.; Chen, D.; Dai, J.; Bialis, T.; Jones, R. A.; Yang, D., Human telomeric sequence forms a hybrid-type intramolecular G-quadruplex structure with mixed parallel/antiparallel strands in potassium solution. *Nucleic Acids Res.* **2006**, *34*, 2723-35.

S12. Phan, A. T.; Modi, Y. S.; Patel, D. J., Propeller-type parallel-stranded G-quadruplexes in the human c-myc promoter. *J. Am. Chem. Soc.* **2004,** *126*, 8710-6.

S13. Dai, J.; Chen, D.; Jones, R. A.; Hurley, L. H.; Yang, D., NMR solution structure of the major G-quadruplex structure formed in the human BCL2 promoter region. *Nucleic Acids Res.* **2006,** *34*, 5133-44.

S14. Rankin, S.; Reszka, A. P.; Huppert, J.; Zloh, M.; Parkinson, G. N.; Todd, A. K.; Ladame, S.; Balasubramanian, S.; Neidle, S., Putative DNA quadruplex formation within the human c-kit oncogene. *J Am Chem Soc* **2005**, *127*, 10584-9.

S15. Fernando, H.; Reszka, A. P.; Huppert, J.; Ladame, S.; Rankin, S.; Venkitaraman, A. R.; Neidle, S.; Balasubramanian, S., A conserved quadruplex motif located in a transcription activation site of the human c-kit oncogene. *Biochemistry* **2006**, *45*, 7854-60.

S16. Perrone, R.; Nadai, M.; Frasson, I.; Poe, J. A.; Butovskaya, E.; Smithgall, T. E.; Palumbo, M.; Palù, G.; Richter, S. N., A Dynamic G-Quadruplex Region Regulates the HIV-1 Long Terminal Repeat Promoter. *Journal of Medicinal Chemistry* **2013**, *56*, 6521-6530.

S17. De Nicola, B.; Lech, C. J.; Heddi, B.; Regmi, S.; Frasson, I.; Perrone, R.; Richter, S. N.; Phan, A. T., Structure and possible function of a G-quadruplex in the long terminal repeat of the proviral HIV-1 genome. *Nucleic Acids Res.* **2016**, *44*, 6442-51.

S18. Artusi, S.; Nadai, M.; Perrone, R.; Biasolo, M. A.; Palu, G.; Flamand, L.; Calistri, A.; Richter, S. N., The Herpes Simplex Virus-1 genome contains multiple clusters of repeated G-quadruplex: Implications for the antiviral activity of a G-quadruplex ligand. *Antiviral Res.* **2015**, *118*, 123-31.

S19. Valko, M.; Jomova, K.; Rhodes, C. J.; Kuca, K.; Musilek, K., Redox- and non-redox-metal-induced formation of free radicals and their role in human disease. *Arch. Toxicol.* **2016**, *90*, 1-37.

S20. Luo, Y.; Henle, E. S.; Linn, S., Oxidative damage to DNA constituents by iron-mediated fenton reactions. The deoxycytidine family. *J. Biol. Chem.* **1996**, *271*, 21167-76.

S21. Fleming, A. M.; Burrows, C. J., G-quadruplex folds of the human telomere sequence alter the site reactivity and reaction pathway of guanine oxidation compared to duplex DNA. *Chem. Res. Toxicol.* **2013**, *26*, 593-607.

S22. Aruoma, O. I.; Halliwell, B.; Gajewski, E.; Dizdaroglu, M., Copper-ion-dependent damage to the bases in DNA in the presence of hydrogen peroxide. *Biochem. J.* **1991**, *273*, 601-4.

S23. Ohyashiki, T.; Nunomura, M.; Katoh, T., Detection of superoxide anion radical in phospholipid liposomal membrane by fluorescence quenching method using 1,3-diphenylisobenzofuran. *Biochim. Biophys. Acta* **1999**, *1421*, 131-9.